specifically binds to the dephosphorylated form of the β-subunit, leading to clathrin-mediated endocytosis of the $GABA_A$ receptor (6–8). Correspondingly, a transient increase and a subsequent long-lasting decrease in I_{GABA} is observed (29, 41). On the other hand, in DKO neurons, BDNF caused a gradual increase in the phosphorylation of the β-subunit and therefore of I_{GABA}, which lasted for the full 30-min examination period (29). Taken together, these results indicate that different extracellular stimuli evoke phosphorylation of the β-subunit of the $GABA_A$ receptor at the same residues via different kinases, the level of which is regulated by the balance of activity between kinase(s) and phosphatase(s) especially in the vicinity of $GABA_A$ receptors but not inside cells. Therefore, the time courses of the phosphorylation level appear to be dependent on the type of stimuli involved. In either case, PRIP through direct association with the $GABA_A$ receptor β-subunit, plays an important role in recruiting proteins including the active form of Akt (this study) and protein phosphatases (PP1 and PP2A) (27, 29), which regulate the phosphorylation of the $GABA_A$ receptor β-subunit, leading to the regulation the number of receptors on the cell surface membrane. In fact, we observed a further decrease of insulin-mediated I_{GABA} below the control level in the BFA-treated WT but not DKO neurons. This observation suggests that insulin elicits both the insertion and subsequent endocytosis of $GABA_A$ receptors and that the balance shifts to membrane insertion in insulin-stimulated WT neurons. The result also suggests that PRIP is involved in both insulin-induced membrane insertion and endocytosis of $GABA_A$ receptors. Other scaffolding molecules such as receptor for activated C kinase-1 (RACK-1) for protein kinase C (47, 48), protein kinase A-anchoring protein (AKAP) 79/150 for cAMP-dependent protein kinase A (PKA) (49), and PRIP (27, 29) have been reported to determine the specificity of the specific kinase(s) or phosphatase(s) recruited to the vicinity of $GABA_A$ receptors. We still do not know the exact molecular mechanisms by which different stimuli regulate the recruitment of kinase(s) and phosphatase(s) to the vicinity of $GABA_A$ receptors. The phosphorylation state of the scaffolding molecules may be one of the pathways that regulates the interaction among these molecules. Additionally, the molecular mechanisms by which phosphorylation of β-subunit triggers the membrane insertion of $GABA_A$ receptors remains largely unknown.

Is there any physiological or pathological relevance of the insulin-induced membrane insertion of $GABA_A$ receptors and the involvement of PRIP? It is reported that oxygen-glucose deprivation (OGD), an ischemia-like challenge, decreases the number of cell surface $GABA_A$ receptors and thereby leads to excitotoxic cell death in cultured hippocampal neurons. Insulin treatment counteracts the OGD-induced diminishment of the number of cell surface $GABA_A$ receptors and thus prevents ischemic cell death (14). Additionally, it is reported that insulin-induced cell surface expression of $GABA_A$ receptors leads to membrane hyperpolarization in islet α cells, thereby suppressing glucagon secretion (12), suggesting its involvement in diabetic pathogenesis. Another example is that interleukin-1β (IL-1β) increases in the cell surface expression of $GABA_A$ receptors depend on the PI 3-kinase-Akt signaling pathway (50). Patients with sepsis-associated encephalopathy (SAE), a neurological complication in sepsis, have higher plasma levels of IL-1β, therefore this may contribute to the cognitive dysfunction observed in SAE by altering GABAergic synaptic strength (50). It is possible that PRIP is implicated in such neuronal dysfunction and pathogenesis through the recruitment of active Akt to $GABA_A$ receptors, suggesting that PRIP could a therapeutic target.

In conclusion, we showed here that PRIP is implicated in the insulin-induced membrane insertion of $GABA_A$ receptors as it recruits active Akt to the vicinity of $GABA_A$ receptors. The subsequent complex formation may serve as the molecular basis for the efficient phosphorylation of $GABA_A$ receptors through Akt and receptor insertion into the cell surface membrane. Therefore, PRIP is a key factor in the control of the plasticity of GABAergic transmission.

Acknowledgments—We thank Dr. U. Kikkawa (Kobe University, Japan) for kindly donating the mammalian expression vector for Akt, pECE/Akt. We thank all of the laboratory members for their critical discussion and reading the manuscript.

REFERENCES

1. Moss, S. J., and Smart, T. G. (2001) *Nat. Rev. Neurosci.* **2,** 240–250
2. Lüscher, B., and Keller, C. A. (2004) *Pharmacol. Ther.* **102,** 195–221
3. Vicini, S., and Ortinski, P. (2004) *Pharmacol. Ther.* **103,** 109–120
4. Michels, G., and Moss, S. J. (2007) *Crit. Rev. Biochem. Mol. Biol.* **42,** 3–14
5. Jacob, T. C., Moss, S. J., and Jurd, R. (2008) *Nat. Rev. Neurosci.* **9,** 331–343
6. Kittler, J. T., Chen, G., Honing, S., Bogdanov, Y., McAinsh, K., Arancibia-Carcamo, I. L., Jovanovic, J. N., Pangalos, M. N., Haucke, V., Yan, Z., and Moss, S. J. (2005) *Proc. Natl. Acad. Sci. U.S.A.* **102,** 14871–14876
7. Chen, G., Kittler, J. T., Moss, S. J., and Yan, Z. (2006) *J. Neurosci.* **26,** 2513–2521
8. Smith, K. R., McAinsh, K., Chen, G., Arancibia-Carcamo, I. L., Haucke, V., Yan, Z., Moss, S. J., and Kittler, J. T. (2008) *Neuropharmacology* **55,** 844–850
9. Kittler, J. T., Chen, G., Kukhtina, V., Vahedi-Faridi, A., Gu, Z., Tretter, V., Smith, K. R., McAinsh, K., Arancibia-Carcamo, I. L., Saenger, W., Haucke, V., Yan, Z., and Moss, S. J. (2008) *Proc. Natl. Acad. Sci. U.S.A.* **105,** 3616–3621
10. Wan, Q., Xiong, Z. G., Man, H. Y., Ackerley, C. A., Braunton, J., Lu, W. Y., Becker, L. E., MacDonald, J. F., and Wang, Y. T. (1997) *Nature* **388,** 686–690
11. Wang, Q., Liu, L., Pei, L., Ju, W., Ahmadian, G., Lu, J., Wang, Y., Liu, F., and Wang, Y. T. (2003) *Neuron.* **38,** 915–928
12. Xu, E., Kumar, M., Zhang, Y., Ju, W., Obata, T., Zhang, N., Liu, S., Wendt, A., Deng, S., Ebina, Y., Wheeler, M. B., Braun, M., and Wang, Q. (2006) *Cell Metab.* **3,** 47–58
13. Vetiska, S. M., Ahmadian, G., Ju, W., Liu, L., Wymann, M. P., and Wang, Y. T. (2007) *Neuropharmacology* **52,** 146–155
14. Mielke, J. G., and Wang, Y. T. (2005) *J. Neurochem.* **92,** 103–113
15. Kanematsu, T., Takeya, H., Watanabe, Y., Ozaki, S., Yoshida, M., Koga, T., Iwanaga, S., and Hirata, M. (1992) *J. Biol. Chem.* **267,** 6518–6525
16. Kanematsu, T., Misumi, Y., Watanabe, Y., Ozaki, S., Koga, T., Iwanaga, S., Ikehara, Y., and Hirata, M. (1996) *Biochem. J.* **313,** 319–325
17. Kanematsu, T., Yoshimura, K., Hidaka, K., Takeuchi, H., Katan, M., and Hirata, M. (2000) *Eur. J. Biochem.* **267,** 2731–2737
18. Matsuda, M., Kanematsu, T., Takeuchi, H., Kukita, T., and Hirata, M. (1998) *Neurosci. Lett.* **257,** 97–100
19. Uji, A., Matsuda, M., Kukita, T., Maeda, K., Kanematsu, T., and Hirata, M. (2002) *Life Sci.* **72,** 443–453
20. Otsuki, M., Fukami, K., Kohno, T., Yokota, J., and Takenawa, T. (1999) *Biochem. Biophys. Res. Commun.* **266,** 97–103

21. Kanematsu, T., Jang, I. S., Yamaguchi, T., Nagahama, H., Yoshimura, K., Hidaka, K., Matsuda, M., Takeuchi, H., Misumi, Y., Nakayama, K., Yamamoto, T., Akaike, N., Hirata, M., and Nakayama, K. (2002) *EMBO. J.* **21,** 1004–1011
22. Mizokami, A., Kanematsu, T., Ishibashi, H., Yamaguchi, T., Tanida, I., Takenaka, K., Nakayama, K. I., Fukami, K., Takenawa, T., Kominami, E., Moss, S. J., Yamamoto, T., Nabekura, J., and Hirata, M. (2007) *J. Neurosci.* **27,** 1692–1701
23. Coyle, J. E., and Nikolov, D. B. (2003) *Neuroscientist* **9,** 205–216
24. Chen, Z. W., and Olsen, R. W. (2007) *J. Neurochem.* **100,** 279–294
25. Yoshimura, K., Takeuchi, H., Sato, O., Hidaka, K., Doira, N., Terunuma, M., Harada, K., Ogawa, Y., Ito, Y., Kanematsu, T., and Hirata, M. (2001) *J. Biol. Chem.* **276,** 17908–17913
26. Yanagihori, S., Terunuma, M., Koyano, K., Kanematsu, T., Ho Ryu, S., and Hirata, M. (2006) *Adv. Enzyme. Regul.* **46,** 203–222
27. Terunuma, M., Jang, I. S., Ha, S. H., Kittler, J. T., Kanematsu, T., Jovanovic, J. N., Nakayama, K. I., Akaike, N., Ryu, S. H., Moss, S. J., and Hirata, M. (2004) *J. Neurosci.* **24,** 7074–7084
28. Kanematsu, T., Fujii, M., Mizokami, A., Kittler, J. T., Nabekura, J., Moss, S. J., and Hirata, M. (2007) *J. Neurochem.* **101,** 898–905
29. Kanematsu, T., Yasunaga, A., Mizoguchi, Y., Kuratani, A., Kittler, J. T., Jovanovic, J. N., Takenaka, K., Nakayama, K. I., Fukami, K., Takenawa, T., Moss, S. J., Nabekura, J., and Hirata, M. (2006) *J. Biol. Chem.* **281,** 22180–22189
30. Kanematsu, T., Takeuchi, H., Terunuma, M., and Hirata, M. (2005) *Mol. Cells* **20,** 305–314
31. Kanematsu, T., Mizokami, A., Watanabe, K., and Hirata, M. (2007) *J. Pharmacol. Sci.* **104,** 285–292
32. Klausner, R. D., Donaldson, J. G., and Lippincott-Schwartz, J. (1992) *J. Cell Biol.* **116,** 1071–1080
33. Chardin, P., and McCormick, F. (1999) *Cell* **97,** 153–155
34. Connolly, C. N., Krishek, B. J., McDonald, B. J., Smart, T. G., and Moss, S. J. (1996) *J. Biol. Chem.* **271,** 89–96
35. Konishi, H., Matsuzaki, H., Tanaka, M., Ono, Y., Tokunaga, C., Kuroda, S., and Kikkawa, U. (1996) *Proc. Natl. Acad. Sci. U.S.A.* **93,** 7639–7643
36. Mizoguchi, Y., Ishibashi, H., and Nabekura, J. (2003) *J. Physiol.* **548,** 703–709
37. Kakazu, Y., Akaike, N., Komiyama, S., and Nabekura, J. (1999) *J. Neurosci.* **19,** 2843–2851
38. Nabekura, J., Ueno, T., Okabe, A., Furuta, A., Iwaki, T., Shimizu-Okabe, C., Fukuda, A., and Akaike, N. (2002) *J. Neurosci.* **22,** 4412–4417
39. Fujii, M., and York, J. D. (2005) *J. Biol. Chem.* **280,** 1156–1164
40. Wang, Q., Somwar, R., Bilan, P. J., Liu, Z., Jin, J., Woodgett, J. R., and Klip, A. (1999) *Mol. Cell. Biol.* **19,** 4008–4018
41. Jovanovic, J. N., Thomas, P., Kittler, J. T., Smart, T. G., and Moss, S. J. (2004) *J. Neurosci.* **24,** 522–530
42. Favre, B., Turowski, P., and Hemmings, B. A. (1997) *J. Biol. Chem.* **272,** 13856–13863
43. Alessi, D. R., and Downes, C. P. (1998) *Biochim. Biophys. Acta.* **1436,** 151–164
44. van der Heide, L. P., Ramakers, G. M., and Smidt, M. P. (2006) *Prog. Neurobiol.* **79,** 205–221
45. Kong, D., and Yamori, T. (2008) *Cancer Sci.* **99,** 1734–1740
46. Goto, H., Terunuma, M., Kanematsu, T., Misumi, Y., Moss, S. J., and Hirata, M. (2005) *Mol. Cell Neurosci.* **30,** 197–206
47. Brandon, N. J., Uren, J. M., Kittler, J. T., Wang, H., Olsen, R., Parker, P. J., and Moss, S. J. (1999) *J. Neurosci.* **19,** 9228–9234
48. Brandon, N. J., Jovanovic, J. N., Smart, T. G., and Moss, S. J. (2002) *J. Neurosci.* **22,** 6353–6361
49. Brandon, N. J., Jovanovic, J. N., Colledge, M., Kittler, J. T., Brandon, J. M., Scott, J. D., and Moss, S. J. (2003) *Mol. Cell Neurosci.* **22,** 87–97
50. Serantes, R., Arnalich, F., Figueroa, M., Salinas, M., Andrés-Mateos, E., Codoceo, R., Renart, J., Matute, C., Cavada, C., Cuadrado, A., and Montiel, C. (2006) *J. Biol. Chem.* **281,** 14632–14643

Oncogene (2010) 29, 1798–1809

www.nature.com/onc

ORIGINAL ARTICLE

Complex regulation of cell-cycle inhibitors by Fbxw7 in mouse embryonic fibroblasts

K Masuda[1,2,3], Y Ishikawa[1,3], I Onoyama[3,4], M Unno[2], IM de Alborán[5], KI Nakayama[3,4] and K Nakayama[1,3]

[1]Department of Developmental Genetics, Center for Translational and Advanced Animal Research, Graduate School of Medicine, Tohoku University, Aoba-ku, Sendai, Japan; [2]Department of Surgery, Graduate School of Medicine, Tohoku University, Aoba-ku, Sendai, Japan; [3]CREST, Japan Science and Technology Agency, Kawaguchi, Saitama, Japan; [4]Department of Molecular and Cellular Biology, Medical Institute of Bioregulation, Kyushu University, Fukuoka, Japan and [5]Department of Immunology and Oncology, National Center for Biotechnology, CNB-CSIC, Madrid, Spain

The F-box protein Fbxw7 (also known as Fbw7, SEL-10, hCdc4 or hAgo) mediates the ubiquitylation and thereby contributes to the degradation of proteins that positively regulate cell cycle. Conditional ablation of *Fbxw7* in mouse embryonic fibroblasts (MEFs) induces cell-cycle arrest accompanied by abnormal accumulation of the intracellular domain of Notch1 (NICD1) and c-Myc. However, the molecular mechanisms by which the accumulation of NICD1 and c-Myc induces cell-cycle arrest have remained unclear. We have now examined the expression of cell-cycle inhibitors in Fbxw7-deficient MEFs and found that the abundance of $p27^{Kip1}$ and $p57^{Kip2}$ is paradoxically decreased. This phenomenon appears to be attributable to the accumulation of NICD1, given that it was recapitulated by overexpression of NICD1 and blocked by ablation of RBP-J. Conversely, the expression of $p16^{Ink4a}$ and $p19^{ARF}$ was increased in an NICD1-independent manner in Fbxw7-null MEFs. The increased expression of $p19^{ARF}$ was recapitulated by overexpression of c-Myc and abolished by ablation of c-Myc, suggesting that the accumulation of c-Myc is primarily responsible for that of $p19^{ARF}$. In contrast, the upregulation of $p16^{Ink4a}$ appeared to be independent of c-Myc. These results indicate that cell-cycle inhibitors undergo complex regulation by the Fbxw7-mediated proteolytic system.
Oncogene (2010) **29,** 1798–1809; doi:10.1038/onc.2009.469; published online 21 December 2009

Keywords: cell cycle; CDK inhibitor; ubiquitin ligase; SCF complex; Notch; conditional knockout mouse

Correspondence: Dr K Nakayama, Department of Developmental Genetics, Center for Translational and Advanced Animal Research, Graduate School of Medicine, Tohoku University, 2-1 Seiryo-machi, Aoba-ku, Sendai 980-8575, Japan.
E-mail: nakayak2@mail.tains.tohoku.ac.jp
Received 10 April 2009; revised 14 November 2009; accepted 19 November 2009; published online 21 December 2009

Introduction

Precise control of the cell cycle is fundamental to regulation of the normal development of multicellular organisms. Indeed, dysregulation of the cell cycle results in developmental defects or tumorigenesis. Proper control of the abundance of positive and negative regulators is required for the ordered progression of the cell cycle and is achieved by both transcriptional and posttranslational mechanisms. Such regulators include cyclins, which modulate the activity of cyclin-dependent kinases (CDKs) and which, together with most other regulators of the cell cycle, undergo specific degradation by the ubiquitin/proteasome system. Two classes of ubiquitin ligase, the anaphase-promoting complex or cyclosome and the Skp1-Cul1/-F-box protein (SCF) complex, are largely responsible for such degradation (Nakayama and Nakayama, 2006).

Fbxw7 (also known as Fbw7, SEL-10, hCdc4 or hAgo) is a member of the F-box family of proteins and was first identified in *Caenorhabditis elegans* as a negative regulator of the signaling protein Notch (LIN-12) (Sundaram and Greenwald, 1993; Hubbard *et al.*, 1997). Fbxw7 functions as the substrate-recognition subunit of an SCF-type ubiquitin ligase complex and targets for degradation various mammalian oncoproteins that promote cell-cycle progression (Nakayama and Nakayama, 2006; Welcker and Clurman, 2008). These targets of Fbxw7 include cyclin E (Koepp *et al.*, 2001; Moberg *et al.*, 2001; Strohmaier *et al.*, 2001), c-Myc (Welcker *et al.*, 2004; Yada *et al.*, 2004) and c-Jun (Nateri *et al.*, 2004).

Given that Fbxw7 is responsible for the degradation of several oncoproteins, it is thought to function as a tumor suppressor. Indeed, mutations in *FBXW7* have been identified in many human cancers, including cholangiocarcinoma, T-cell acute lymphoblastic leukemia, endometrial cancer and colon cancer (Nakayama and Nakayama, 2006; Akhoondi *et al.*, 2007; Welcker and Clurman, 2008). Moreover, the *FBXW7* locus maps to human chromosomal region 4q32, which is frequently deleted in a wide range of human tumor types (Knuutila *et al.*, 1999).

Mice lacking Fbxw7 manifest marked accumulation of Notch and die *in utero* at embryonic day 10.5 showing abnormalities of vascular development caused by deregulation of Notch signaling (Tetzlaff *et al.*, 2004; Tsunematsu *et al.*, 2004). *Fbxw7*$^{+/-}$ mice show an increased susceptibility to radiation-induced tumorigenesis, although most tumors retain the wild-type allele (Mao *et al.*, 2004). In addition, c-Myc was found to accumulate in *Fbxw7*$^{-/-}$ embryonic stem cells (Yada *et al.*, 2004). To avoid the embryonic mortality of conventional *Fbxw7*$^{-/-}$ mice, we generated mice with conditional inactivation of *Fbxw7* in various tissues (Onoyama *et al.*, 2007). Disruption of *Fbxw7* in the T-cell lineage resulted in accumulation of Notch1 and c-Myc, which was shown to be responsible for the development of thymic hyperplasia and lymphoma in the affected animals (Onoyama *et al.*, 2007). In addition, inactivation of Fbxw7 in hematopoietic stem cells induced activation of the cell cycle as a result of the accumulation of c-Myc, leading to the premature loss of these cells (Matsuoka *et al.*, 2008; Thompson *et al.*, 2008). We have also previously shown that ablation of Fbxw7 in mouse embryonic fibroblasts (MEFs) induced cell-cycle arrest and apoptosis, even though Fbxw7 is considered a negative regulator of the cell cycle and a tumor suppressor (Ishikawa *et al.*, 2008). Although these phenotypes were found to be largely attributable to Notch1 accumulation and to be dependent in part on p53, the precise mechanism underlying the cell-cycle arrest in Fbxw7-deficient (*Fbxw7*$^{\Delta/\Delta}$) MEFs has remained unclear.

We now show that inactivation of *Fbxw7* in MEFs results both in downregulation of the CDK inhibitors (CKIs) p27^{Kip1} and p57^{Kip2} in a manner dependent on the activation of Notch signaling as well as in upregulation of the tumor suppressor proteins p16^{Ink4a} and p19^{ARF} in a manner dependent in part on the accumulation of c-Myc. The results of our study thus reveal a complex mechanism of cell-cycle regulation through Fbxw7-mediated protein degradation.

Results

Notch-dependent downregulation of p27^{Kip1} *and p57*^{Kip2} *in* Fbxw7$^{\Delta/\Delta}$ *MEFs*

We have previously shown that the inhibition of cell-cycle progression apparent in *Fbxw7*$^{\Delta/\Delta}$ MEFs is largely attributable to accumulation of the intracellular domain of Notch1 (NICD1), which is a substrate of Fbxw7 (Ishikawa *et al.*, 2008). Although NICD1 accumulation results in activation of a p53-dependent pathway that upregulates the CKI p21^{Cip1} in *Fbxw7*$^{\Delta/\Delta}$ MEFs (Ishikawa *et al.*, 2008), ablation of p53 did not fully revert the phenotype of these cells, suggesting that a pathway (or pathways) other than the p53/p21^{Cip1} axis contributes to the cell-cycle arrest. We therefore examined the expression of the CKIs p27^{Kip1} and p57^{Kip2} in *Fbxw7*$^{\Delta/\Delta}$ MEFs. Immunoblot analysis revealed that the abundance of both p27^{Kip1} and p57^{Kip2} was increased in response to serum deprivation in wild-type (*Fbxw7*$^{+/+}$) or *Fbxw7*$^{F/F}$ MEFs. Unexpectedly, however, such upregulation of these CKIs was not observed in *Fbxw7*$^{\Delta/\Delta}$ MEFs (Figure 1a).

To examine whether this reduced expression of p27^{Kip1} and p57^{Kip2} in *Fbxw7*$^{\Delta/\Delta}$ MEFs is attributable to NICD1 accumulation, we adopted a genetic approach. Mammalian members of the Notch family of proteins interact with the DNA binding protein RBP-J, and the resulting complex usually behaves as a transcriptional activator (Kato *et al.*, 1996; Artavanis-Tsakonas *et al.*, 1999). To examine the possibility that the NICD1/RBP-J complex functions as a transcriptional repressor for *p27* and *p57* genes, we crossed *Fbxw7*$^{F/F}$ mice with *Rbpj*$^{F/F}$ mice (Han *et al.*, 2002), and then generated *Fbxw7*$^{+/+}$*Rbpj*$^{\Delta/\Delta}$ and *Fbxw7*$^{\Delta/\Delta}$*Rbpj*$^{\Delta/\Delta}$ MEFs by infecting *Fbxw7*$^{+/+}$*Rbpj*$^{F/F}$ or *Fbxw7*$^{F/F}$*Rbpj*$^{F/F}$ MEFs with a retrovirus encoding Cre recombinase. We confirmed by PCR analysis that the floxed alleles of both *Fbxw7* and *Rbpj* were deleted in the infected cells (data not shown). The ablation of RBP-J in Fbxw7-null MEFs largely restored the expression of both p27^{Kip1} and p57^{Kip2} apparent after serum deprivation to the levels observed in *Fbxw7*$^{+/+}$*Rbpj*$^{+/+}$ or *Fbxw7*$^{+/+}$*Rbpj*$^{\Delta/\Delta}$ MEFs (Figure 1b), suggesting that the Notch signaling pathway, which is abnormally activated in *Fbxw7*$^{\Delta/\Delta}$ MEFs, suppresses the expression of p27^{Kip1} and p57^{Kip2} induced by serum deprivation. The levels of p27^{Kip1} and p57^{Kip2} were not increased in *Fbxw7*$^{+/+}$*Rbpj*$^{\Delta/\Delta}$ MEFs compared with *Fbxw7*$^{+/+}$*Rbpj*$^{+/+}$ cells, suggesting that Notch1/RBP-J pathway is not so active in the wild-type cells but is highly active in *Fbxw7*$^{\Delta/\Delta}$ MEFs. Similar results were obtained by siRNA-mediated depletion of Notch1 in *Fbxw7*$^{\Delta/\Delta}$ MEFs (Figure 1c), suggesting that Notch1, but not other Notch family proteins, is the main suppressor for the expression of p27^{Kip1} and p57^{Kip2}. We also measured p27^{Kip1} and p57^{Kip2} mRNA levels in serum-deprived MEFs of the various genotypes and found that the amount of p27^{Kip1} mRNA was decreased in *Fbxw7*$^{\Delta/\Delta}$*Rbpj*$^{+/+}$ MEFs compared with that in *Fbxw7*$^{+/+}$*Rbpj*$^{+/+}$ MEFs, and that this difference was largely abolished by ablation of RBP-J in the Fbxw7-deficient cells (Figure 1d). In contrast, the suppression of p57^{Kip2} mRNA in *Fbxw7*$^{\Delta/\Delta}$*Rbpj*$^{+/+}$ MEFs was more pronounced than that of p27^{Kip1} mRNA, and it was only partially reversed in *Fbxw7*$^{\Delta/\Delta}$*Rbpj*$^{\Delta/\Delta}$ MEFs. These results suggested that increased Notch signaling in *Fbxw7*$^{\Delta/\Delta}$*Rbpj*$^{+/+}$ MEFs suppresses both p27^{Kip1} expression and p57^{Kip2} expression and that these effects are attributable, at least in part, to inhibition of p27^{Kip1} and p57^{Kip2} gene transcription.

Suppression of p27^{Kip1} *and p57*^{Kip2} *expression by Notch signaling*

To examine whether the increased level of NICD1 alone is sufficient to inhibit the expression of p27^{Kip1} and p57^{Kip2}, we infected wild-type MEFs with a retrovirus encoding NICD1. Immunoblot analysis revealed that overexpression of NICD1 resulted in a marked decrease in the abundance of p27^{Kip1} and p57^{Kip2} in asynchronous

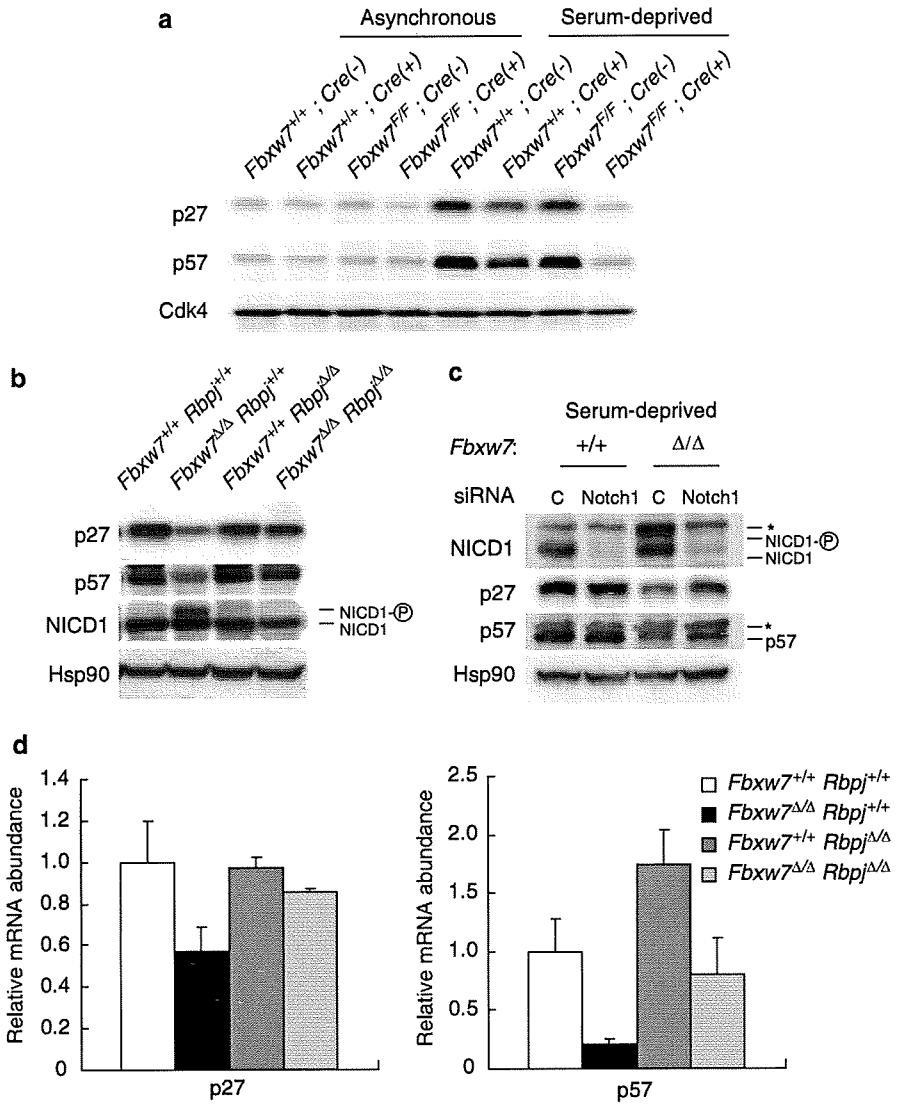

Figure 1 Suppression of p27^{Kip1} and p57^{Kip2} expression through activation of Notch signaling in Fbxw7-deficient mouse embryonic fibroblasts (MEFs). (**a**) Asynchronous or serum-deprived *Fbxw7*$^{+/+}$ (infected or not with a retrovirus for Cre recombinase), *Fbxw7*$^{F/F}$ or *Fbxw7*$^{\Delta/\Delta}$ MEFs were lysed and subjected to immunoblot analysis with antibodies to p27^{Kip1}, p57^{Kip2} or Cdk4 (loading control). (**b**) Serum-deprived MEFs of the indicated genotypes were lysed and subjected to immunoblot analysis with antibodies to p27^{Kip1}, p57^{Kip2}, Notch1 and Hsp90 (loading control). The positions of phosphorylated (P) and nonphosphorylated forms of NICD1 are indicated. The positions of nonspecific bands (*) are indicated. (**c**) Serum-deprived MEFs of the indicated genotypes transfected with a control (C) or *Notch1* siRNA were subjected to immunoblot analysis with antibodies to NICD1, p27^{Kip1}, p57^{Kip2} or Hsp90 (loading control). The positions of nonspecific bands (*) are indicated. (**d**) Serum-deprived MEFs of the indicated genotypes were subjected to quantitative RT-PCR analysis of p27^{Kip1} and p57^{Kip2} mRNAs. Data are means ± s.d. of at least triplicates from a representative experiment.

or serum-deprived cells (Figure 2a) and that this effect was accompanied by a marked increase in the amount of HeyL mRNA (Figure 2b), a target gene of the NICD/RBP-J complex. Overexpression of NICD1 did not affect the abundance of the mRNA for Skp2 (Figure 2b), a component of the SCF^{Skp2} complex that functions as a ubiquitin ligase for p27^{Kip1} and p57^{Kip2}, even though the *Skp2* gene has been identified as a target of Notch1 (Sarmento *et al*., 2005). Forced expression of NICD1 also reduced the amounts of p27^{Kip1} and p57^{Kip2} mRNAs (Figure 2c). These results, together with those presented in Figure 1, suggested that the accumulation of NICD1 is both required and sufficient for the suppression of p27^{Kip1} and p57^{Kip2} expression.

Accumulation of p16^{Ink4a} *and p19*^{ARF} *in* Fbxw7$^{\Delta/\Delta}$ *MEFs*

We next examined the expression of p16^{Ink4a} and p19^{ARF} and found that the amounts of both the proteins are increased in asynchronous *Fbxw7*$^{\Delta/\Delta}$ MEFs compared with those in asynchronous *Fbxw7*$^{+/+}$ or *Fbxw7*$^{+/\Delta}$ MEFs (Figure 3a). To investigate whether this upregulation of p16^{Ink4a} and p19^{ARF} is dependent on the accumulation of NICD1 in *Fbxw7*$^{\Delta/\Delta}$ MEFs, we examined their expression in *Fbxw7*$^{\Delta/\Delta}$*Rbpj*$^{\Delta/\Delta}$ MEFs. Immunoblot analysis revealed that the upregulation of p16^{Ink4a} and p19^{ARF} was not affected by disruption of RBP-J-dependent Notch signaling (Figure 3b). The abundance of p16^{Ink4a} and p19^{ARF} mRNAs was also increased in *Fbxw7*$^{\Delta/\Delta}$ MEFs as well as in *Fbxw7*$^{\Delta/\Delta}$*Rbpj*$^{\Delta/\Delta}$

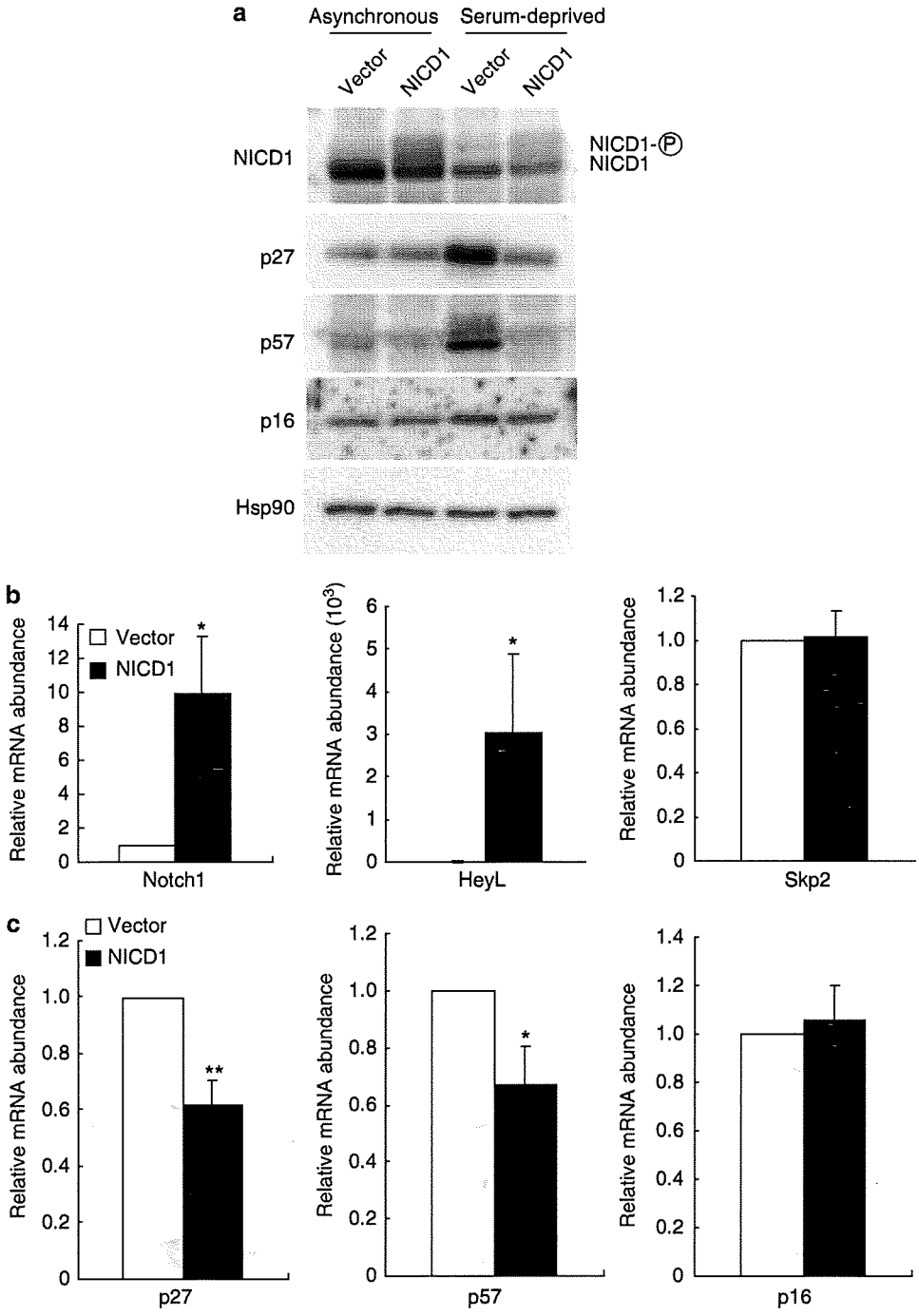

Figure 2 Suppression of p27^{Kip1} and p57^{Kip2} expression by Notch signaling in mouse embryonic fibroblasts (MEFs). (**a**) Asynchronous or serum-deprived wild-type MEFs infected with a retrovirus encoding NICD1 or with the corresponding empty vector were subjected to immunoblot analysis with antibodies to NICD1, p27^{Kip1}, p57^{Kip2} or p16^{Ink4}. (**b**, **c**) Quantitative RT–PCR analysis of Notch1, HeyL and Skp2 mRNAs (**b**) or of p27^{Kip1}, p57^{Kip2} and p16^{Ink4a} mRNAs (**c**) in asynchronous wild-type MEFs infected as in **a**. Data are means ± s.d. of at least triplicates from representative experiments. *$P<0.05$, **$P<0.01$ versus the corresponding value for cells infected with the empty vector.

MEFs (Figure 3c). Furthermore, overexpression of NICD1 did not affect p16^{Ink4a} at either protein or mRNA level (Figures 2a and c). These results suggested that the transcription of p16^{Ink4a} and p19^{ARF} genes is increased in *Fbxw7*$^{\Delta/\Delta}$ MEFs in a Notch-independent manner.

Given that a high level of c-Myc expression was previously shown to induce p19^{ARF} expression (Zindy *et al.*, 1998) and that c-Myc is a target of the SCF^{Fbxw7} ubiquitin ligase, we examined the abundance of c-Myc in *Fbxw7*$^{\Delta/\Delta}$ MEFs. Immunoblot analysis revealed that the amount of c-Myc was slightly higher in *Fbxw7*$^{\Delta/\Delta}$

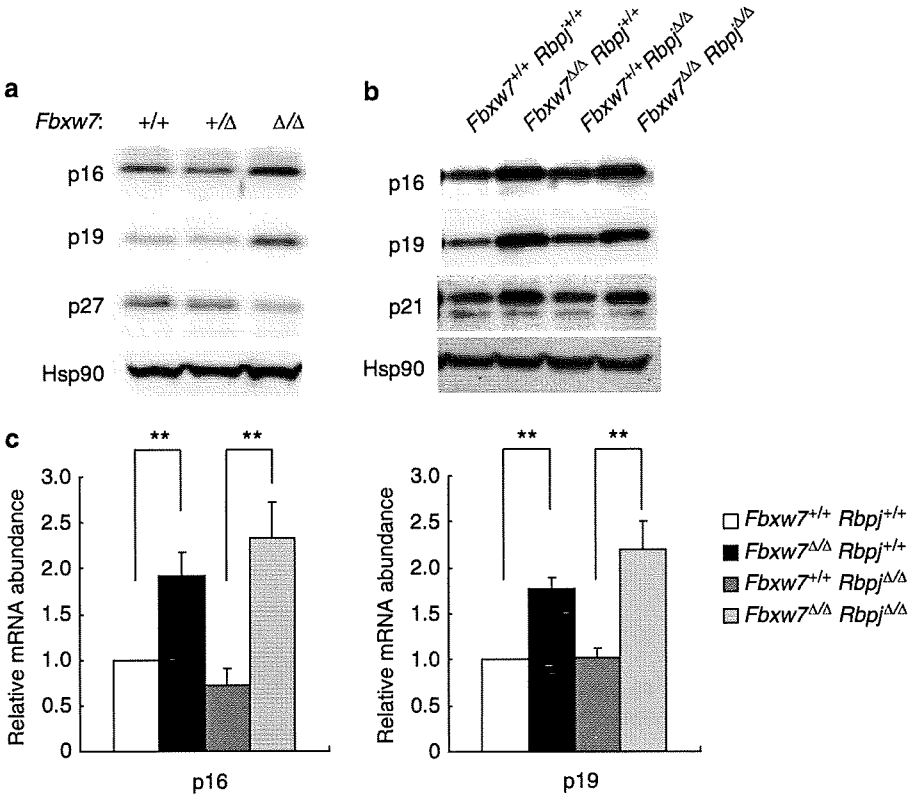

Figure 3 Increased expression of p16^{Ink4a} and p19^{ARF} induced by Fbxw7 deficiency independently of Notch signaling. (**a**) Immunoblot analysis of p16^{Ink4a}, p19^{ARF} and p27^{Kip1} in asynchronous *Fbxw7*$^{+/+}$, *Fbxw7*$^{+/\Delta}$ and *Fbxw7*$^{\Delta/\Delta}$ mouse embryonic fibroblasts (MEFs). (**b**) Immunoblot analysis of p16^{Ink4a}, p19^{ARF} and p21^{Cip1} in asynchronous MEFs of the indicated genotypes. (**c**) Quantitative RT–PCR analysis of p16^{Ink4a} and p19^{ARF} mRNAs in asynchronous MEFs of the indicated genotypes. Data are means ± s.d. of at least triplicates from a representative experiment. $^{**}P<0.01$.

MEFs than in *Fbxw7*$^{+/+}$ MEFs and that this difference was more pronounced in the absence of p53 (Figure 4a), probably because ablation of p53 results in a partial recovery from cell-cycle arrest in *Fbxw7*$^{\Delta/\Delta}$ MEFs and thereby increases c-Myc expression (Ishikawa *et al.*, 2008). The expression of p16^{Ink4a} and p19^{ARF} appeared to be proportional to that of c-Myc in *Fbxw7*$^{+/+}$*p53*$^{-/-}$ and *Fbxw7*$^{\Delta/\Delta}$*p53*$^{-/-}$ MEFs (Figure 4a, right panel), suggesting that c-Myc accumulation might be responsible for the upregulation of p16^{Ink4a} and p19^{ARF} in the Fbxw7-deficient cells. Given that deletion of *Fbxw7* had no effect on the amount of c-Myc mRNA (Figure 4b), Fbxw7 likely regulates the abundance of c-Myc at the protein level. Indeed, we confirmed that the stability of endogenous c-Myc is increased in *Fbxw7*$^{\Delta/\Delta}$ MEFs with the use of a cycloheximide chase assay (Figure 4c).

Upregulation of p19^{ARF} *induced by overexpression of c-Myc*

To determine whether overexpression of c-Myc in wild-type MEFs might recapitulate the accumulation of p16^{Ink4a} and p19^{ARF} observed in *Fbxw7*$^{\Delta/\Delta}$ MEFs, we infected the wild-type cells with a retrovirus encoding c-Myc. Overexpression of c-Myc promoted cell proliferation (Figure 5a) as well as increased the percentage of cells in S phase of the cell cycle (Figure 5b). It also increased the proportion of apoptotic cells, which were detected by flow cytometry either as cells with a sub-G_1 DNA content or as those stained with annexin V (Figure 5b). Forced expression of c-Myc increased the expression of p19^{ARF} at both the mRNA and protein levels, whereas it did not affect the amount of p16^{Ink4a} protein and actually reduced the amount of p16^{Ink4a} mRNA (Figures 5c and d). The abundance of p27^{Kip1} was not affected by c-Myc overexpression (Figure 5c). These results suggested that the increased expression of c-Myc in *Fbxw7*$^{\Delta/\Delta}$ MEFs is responsible for the upregulation of p19^{ARF} but not for that of p16^{Ink4a}.

c-Myc dependence of p19^{ARF} *upregulation in* Fbxw7$^{\Delta/\Delta}$ *MEFs*

To examine further whether the increased expression of p19^{ARF} in *Fbxw7*$^{\Delta/\Delta}$ MEFs is attributable to the accumulation of c-Myc, we crossed *Fbxw7*$^{F/F}$ mice with *c-Myc*$^{F/F}$ mice (de Alboran *et al.*, 2004). *Fbxw7*$^{F/F}$ *c-Myc*$^{F/F}$ MEFs prepared from the resulting offspring were infected with a retrovirus encoding Cre recombinase to generate *Fbxw7*$^{\Delta/\Delta}$*c-Myc*$^{\Delta/\Delta}$ cells. Immunoblot analysis showed that the increased p19^{ARF} expression apparent in *Fbxw7*$^{\Delta/\Delta}$ MEFs was not observed in *Fbxw7*$^{\Delta/\Delta}$*c-Myc*$^{\Delta/\Delta}$ MEFs (Figures 6a and b). We also found that both p53 and p21^{Cip1} were increased in

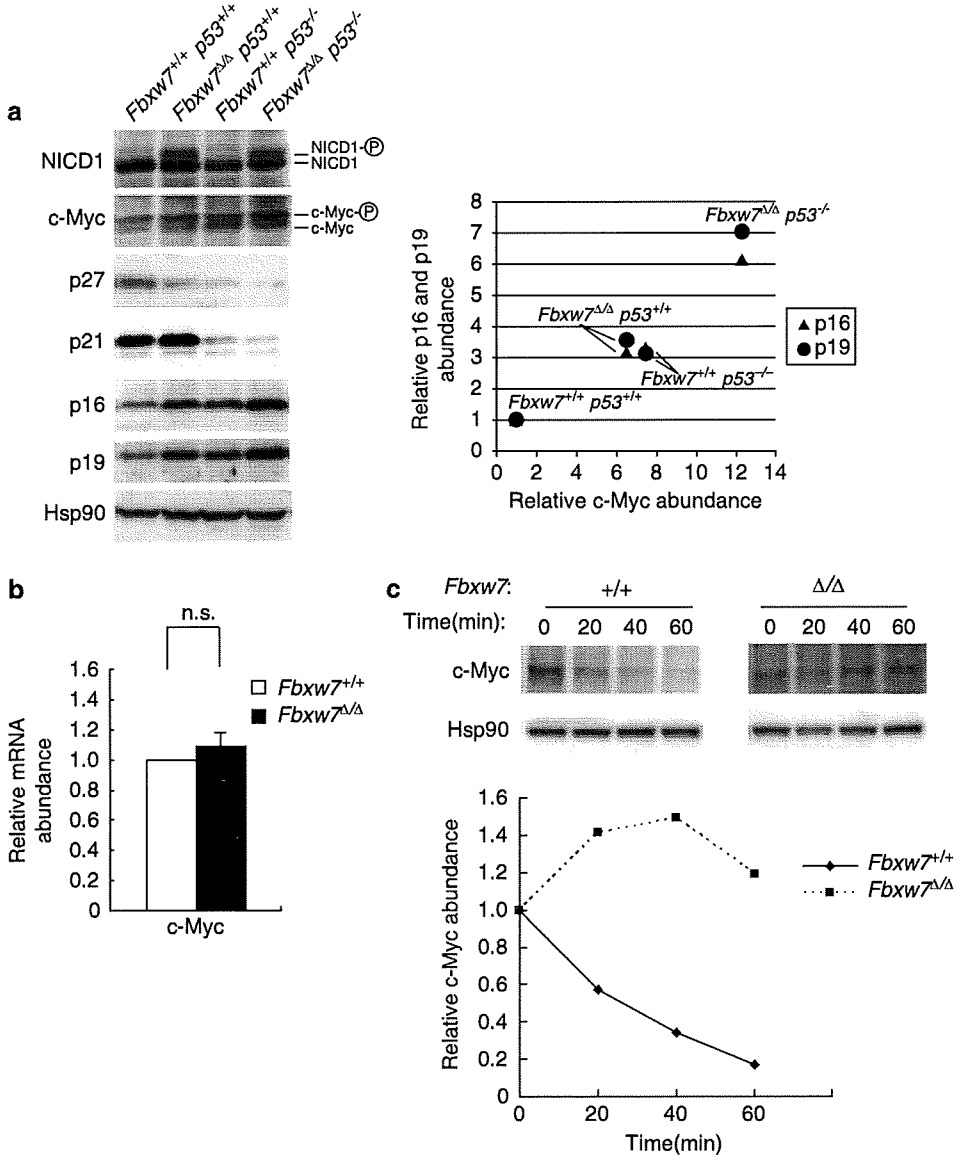

Figure 4 Accumulation of c-Myc in Fbxw7-deficient mouse embryonic fibroblasts (MEFs). (**a**) Immunoblot analysis of c-Myc and the indicated proteins in asynchronous MEFs of the indicated genotypes. The positions of phosphorylated (P) and nonphosphorylated forms of NICD1 and c-Myc are indicated. The amount of c-Myc, p16^{Ink4a} and p19^{ARF} in each genotype to *Fbxw7*$^{+/+}$*c-Myc*$^{+/+}$ was quantified by image analysis and normalized by the amount of *Fbxw7*$^{+/+}$*c-Myc*$^{+/+}$ (right panel). (**b**) Quantitative RT–PCR analysis of c-Myc mRNA in asynchronous wild-type and *Fbxw7*$^{\Delta/\Delta}$ MEFs. Data are means ± s.d. of at least triplicates from a representative experiment. NS, not significant. (**c**) The amount of c-Myc in *Fbxw7*$^{+/+}$ and *Fbxw7*$^{\Delta/\Delta}$ MEFs during exposure of the cells to cycloheximide for the indicated times was monitored by immunoblot analysis (upper panels). The relative amount of c-Myc remaining at each time point was quantified by image analysis and normalized by the amount of Hsp90 (lower panel).

Fbxw7$^{\Delta/\Delta}$ MEFs, and these increases were abolished by the additional deletion of c-Myc. However, overexpression of c-Myc alone did not result in the increase in p21^{Cip1} abundance (Figure 5c), suggesting that both Notch1 and c-Myc pathways are required for the increase in p21^{Cip1}. Analyses for cell cycle and apoptosis in wild-type, *Fbxw7*$^{\Delta/\Delta}$ and *Fbxw7*$^{\Delta/\Delta}$*c-Myc*$^{\Delta/\Delta}$ MEFs revealed that c-Myc was essential for efficient progress of the cell cycle and loss of c-Myc resulted in pronounced arrest of the cell cycle and induction of apoptosis regardless of normalization of p19^{ARF} level (Figure 6c). The stability of p19^{ARF} as revealed by cycloheximide chase analysis was markedly increased in *Fbxw7*$^{\Delta/\Delta}$ MEFs compared with that in wild-type cells, but such stabilization of p19^{ARF} was not apparent in *Fbxw7*$^{\Delta/\Delta}$*c-Myc*$^{\Delta/\Delta}$ MEFs (Figure 6d). The upregulation of p19^{ARF} in *Fbxw7*$^{\Delta/\Delta}$ MEFs therefore seems to be mediated at both transcriptional and posttranslational levels. Moreover, the increases in the amounts of p53 and p21^{Cip1} observed in *Fbxw7*$^{\Delta/\Delta}$ MEFs were abolished by ablation of c-Myc (Figures 6a and b), suggesting that the p53/p21^{Cip1} pathway operates downstream of c-Myc. Given that the p53/p21^{Cip1} pathway is also regulated by Notch1 (Ishikawa *et al.*, 2008), Fbxw7 appears to control this pathway through both Notch1 and c-Myc (Figure 7).

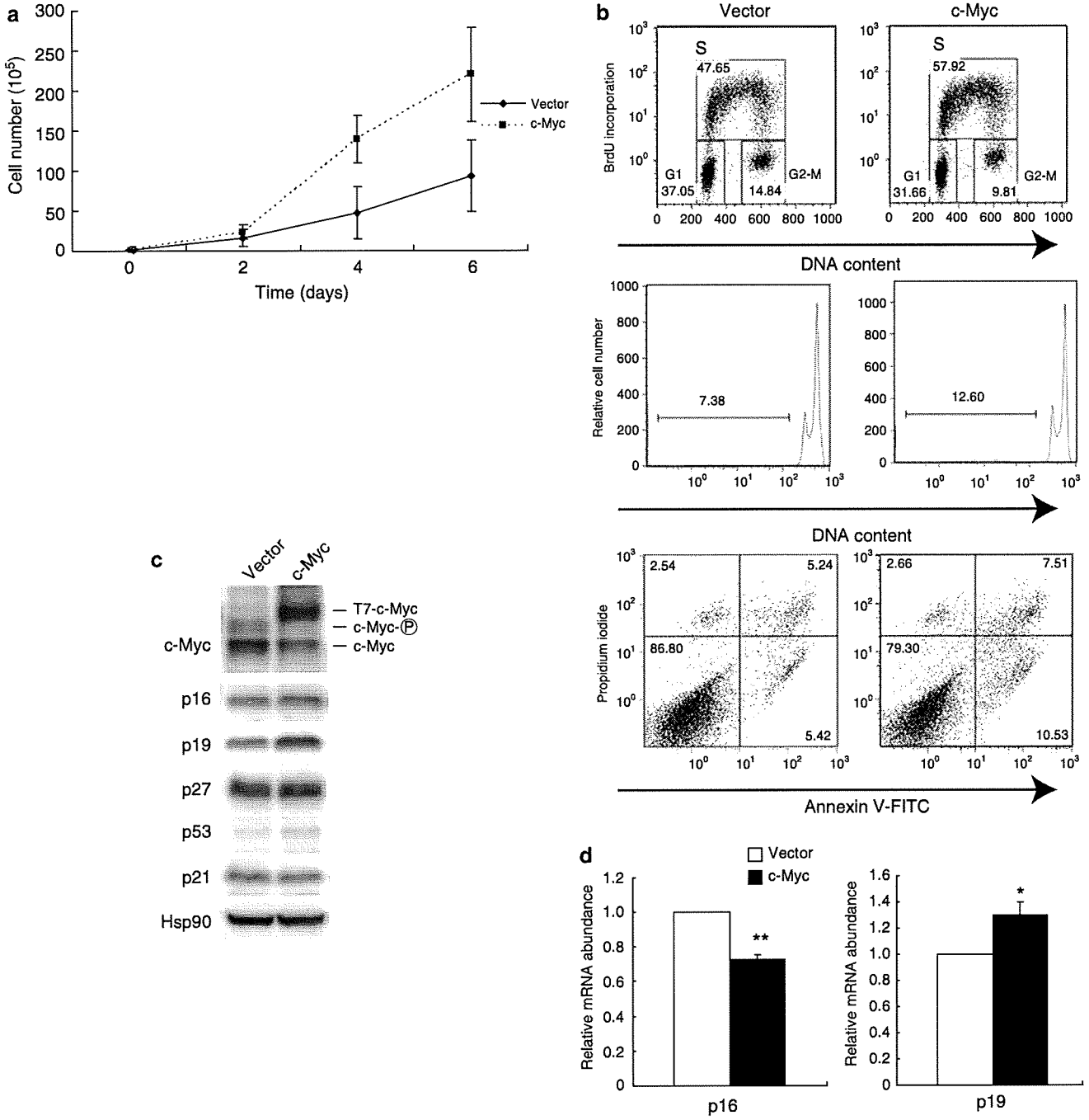

Figure 5 Induction of p19^{ARF} expression in mouse embryonic fibroblasts (MEFs) by overexpression of c-Myc. (**a**) Growth curves for wild-type MEFs infected with a retrovirus encoding c-Myc or with the corresponding empty vector. Data are means ± s.d. of at least triplicates from a representative experiment. (**b**) MEFs infected as in **a** were labeled with bromodeoxyuridine (BrdU) and stained with propidium iodide, and cells with a DNA content of 2C or 4C were counted using flow cytometry. The percentages of cells in G_1, S and G_2–M phases of the cell cycle are indicated (upper panels). The incidence of apoptosis in the MEFs was also determined by flow cytometric analysis of cells with a DNA content of <2C (middle panels) or of those stained with annexin V–fluorescein isothiocyanate (FITC) and counterstained with propidium iodide (lower panels). (**c**) Immunoblot analysis of c-Myc, p16^{Ink4a}, p19^{ARF} and the indicated proteins in MEFs infected as in **a**. Exogenous c-Myc protein is indicated by T7-c-Myc. (**d**) Quantitative RT-PCR analysis of p16^{Ink4a} and p19^{ARF} mRNAs in MEFs infected as in (**a**). Data are means ± s.d. of at least triplicates from a representative experiment. *$P<0.05$, **$P<0.01$ versus the corresponding value for cells infected with the empty vector.

Discussion

With genetic approaches, we and others have shown that Fbxw7 controls various cell-cycle regulators either directly or indirectly in a tissue-specific manner (Tetzlaff *et al.*, 2004; Tsunematsu *et al.*, 2004; Onoyama *et al.*, 2007; Ishikawa *et al.*, 2008; Matsuoka *et al.*, 2008; Onoyama and Nakayama, 2008; Thompson *et al.*,

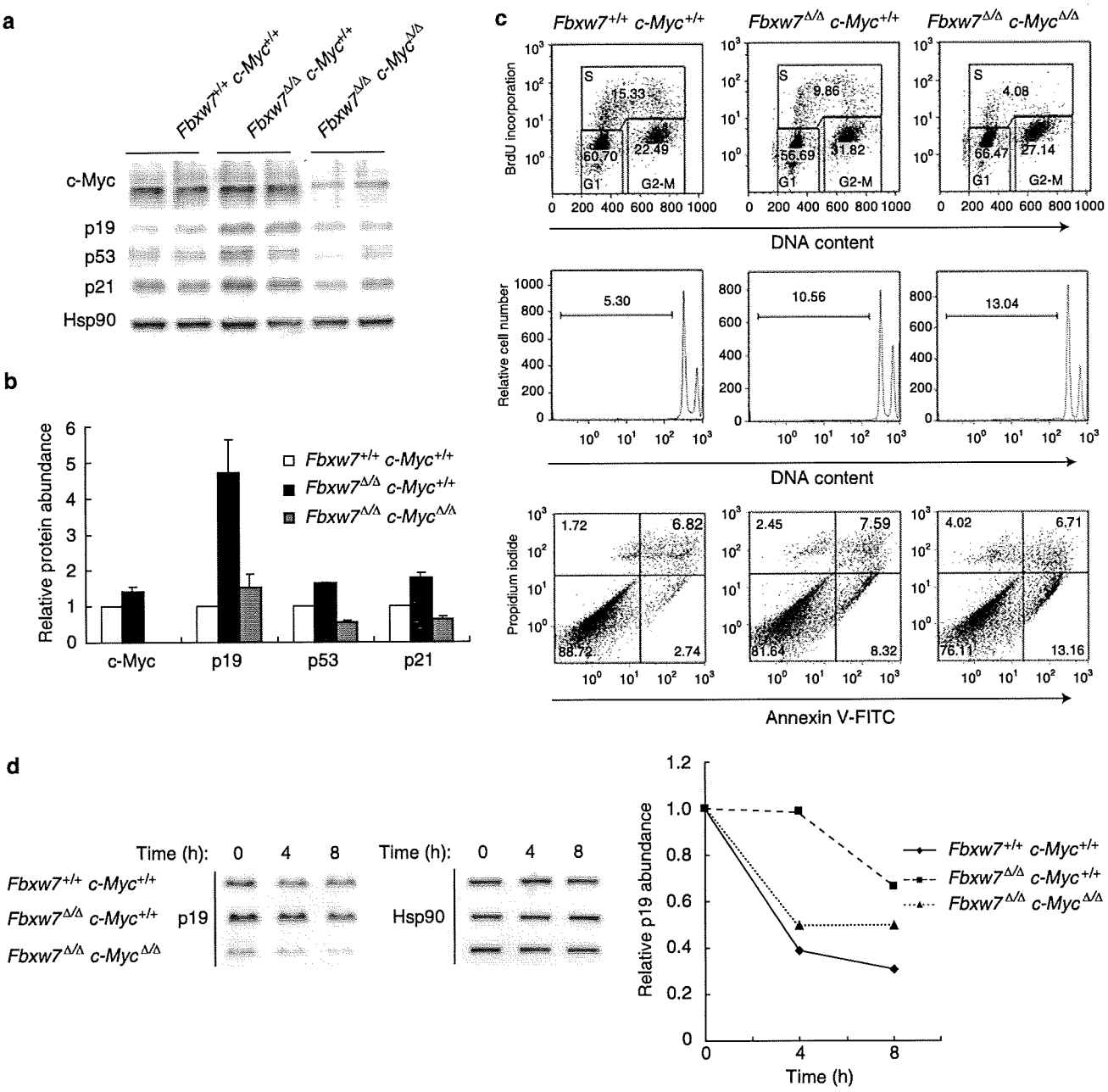

Figure 6 c-Myc dependence of p19^{ARF} upregulation in *Fbxw7*$^{\Delta/\Delta}$ mouse embryonic fibroblasts (MEFs). (**a**) MEFs of the indicated *Fbxw7* and *c-Myc* genotypes were infected with a retrovirus encoding Cre recombinase. Immunoblot analysis of c-Myc, p19^{ARF}, p53 and p21^{Cip1} in MEFs of the indicated genotypes. Given that the MEFs were prepared from mouse embryos that were not in a litter, we show double lanes for each genotypes to show the reproducibility of the results regardless of the MEF lines. (**b**) The relative amount of c-Myc, p19^{ARF}, p53 and p21^{Cip1} protein was quantified by image analysis and normalized by the amount of Hsp90. (**c**) MEFs infected as in **a** were labeled with bromodeoxyuridine (BrdU) and stained with propidium iodide, and cells with a DNA content of 2C or 4C were counted by flow cytometry. The percentages of cells in G_1, S and G_2–M phases of the cell cycle are indicated (upper panels). The incidence of apoptosis in the MEFs was also determined by flow cytometric analysis of cells with a DNA content of <2C (middle panels) or of those stained with annexin V–fluorescein isothiocyanate (FITC) and counterstained with propidium iodide (lower panels). (**d**) Immunoblot analysis of p19^{ARF} in *Fbxw7*$^{+/+}$*c-Myc*$^{+/+}$, *Fbxw7*$^{\Delta/\Delta}$*c-Myc*$^{+/+}$ and *Fbxw7*$^{\Delta/\Delta}$*c-Myc*$^{\Delta/\Delta}$ MEFs at the indicated times of exposure to cycloheximide (left panels). The relative amount of p19^{ARF} remaining at the various chase times was quantified by image analysis and normalized by the amount of Hsp90 (right panel).

2008). In contrast to our expectation that Fbxw7 loss would confer a growth advantage, it induced cell-cycle arrest and apoptosis in MEFs (Ishikawa *et al.*, 2008). Although we have previously shown that the major physiological target of Fbxw7 in MEFs is the NICD1/p53 pathway, the activation of this pathway was not sufficient to explain all the observed characteristics of Fbxw7-null MEFs. We have now explored in more detail the mechanisms responsible for the cell-cycle arrest and apoptosis in *Fbxw7*$^{\Delta/\Delta}$ MEFs.

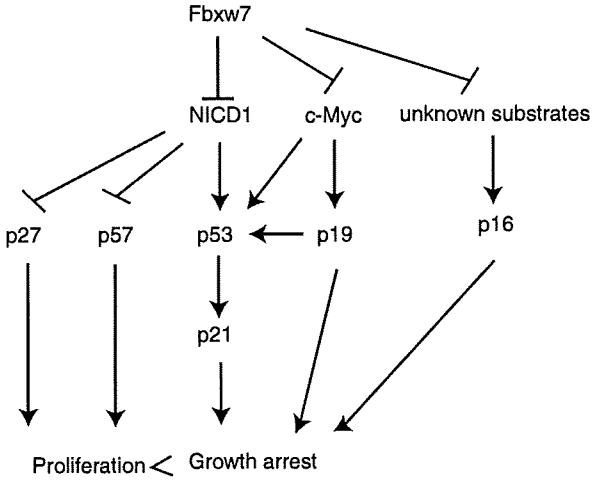

Figure 7 Pathways for the control of cell-cycle regulators by Fbxw7. The expression of p27^{Kip1} and p57^{Kip2} is regulated by Fbxw7 through the degradation of NICD1. Loss of Fbxw7 results in aberrant activation of NICD1 pathway, which in turn suppresses the expression of p27^{Kip1} and p57^{Kip2} but increases that of p53 and p21^{Cip1}. The expression of p19^{ARF} is dependent on c-Myc. The amount of p16^{Ink4a} increases by the deletion of Fbxw7 through neither NICD1 nor c-Myc, suggesting that other unknown substrates of Fbxw7 might be involved in this increase.

The level of p27^{Kip1} in cells is a determinant of the balance between proliferation versus quiescence. The expression of this CKI is increased in cells subjected to mitogen deprivation or otherwise rendered quiescent (Coats *et al.*, 1996; Besson *et al.*, 2007). Similarly, the expression of p57^{Kip2} is increased in serum-deprived osteoblasts (Urano *et al.*, 1999) or MEFs (Kamura *et al.*, 2003). We have now shown that the expression of p27^{Kip1} and p57^{Kip2} is decreased in *Fbxw7*$^{\Delta/\Delta}$ MEFs compared with that in wild-type cells. Furthermore, this effect of Fbxw7 deficiency was not apparent in the absence of RBP-J. Notch1 was previously shown to induce the expression of Skp2, an F-box protein that mediates the ubiquitin-dependent proteolysis of p27^{Kip1} and p57^{Kip2}, with this effect being mediated at the transcriptional level and resulting in the degradation of p27^{Kip1} in 3T3 mouse fibroblasts (Sarmento *et al.*, 2005). However, the reduced expression of p27^{Kip1} and p57^{Kip2} in *Fbxw7*$^{\Delta/\Delta}$ MEFs was also apparent at the mRNA level. Moreover, the induction of Skp2 mRNA was not apparent either in *Fbxw7*$^{\Delta/\Delta}$ MEFs (data not shown) or in wild-type MEFs expressing exogenous NICD1 (Figure 2b). These results thus exclude the possibility that upregulation of Skp2 induced by the accumulation of NICD1 is primarily responsible for the downregulation of p27^{Kip1} and p57^{Kip2} observed in *Fbxw7*$^{\Delta/\Delta}$ MEFs.

Notch signaling has been implicated in repression of the expression of p27^{Kip1} and p57^{Kip2} at the transcriptional level. In *Xenopus*, for example, increased Notch signaling results in inhibition of transcription of the gene for Xic1, the frog orthologue of p27^{Kip1}, in the neural plate, an effect that contributes to regulation of the differentiation of primary neurons (Vernon *et al.*, 2006). In mouse intestinal crypt progenitor cells, Hairy/enhancer of split 1 (Hes1), a well-characterized target of Notch signaling, inhibits transcription of the genes for both p27^{Kip1} and p57^{Kip2}, contributing to maintenance of the proliferative crypt compartment of the small intestine (Riccio *et al.*, 2008). Furthermore, induction of Hes1 resulted in direct inhibition of the activity of the p27^{Kip1} gene promoter, with this effect being mediated by the binding of Hes1 to a class C binding site in the promoter region (Murata *et al.*, 2005). Transcription of the p57^{Kip2} gene is also regulated by Hes1 in the pancreas (Georgia *et al.*, 2006). In addition, the related transcriptional repressor Hey1 (hairy/enhancer-of-split related with YRPW motif 1), which is also activated by Notch, controls the size of the ocular lens by directly suppressing p57^{Kip2} expression (Jia *et al.*, 2007). These various observations suggest that NICD1 or its downstream transcriptional repressors might be responsible for transcriptional inhibition of the p27^{Kip1} and p57^{Kip2} genes in *Fbxw7*$^{\Delta/\Delta}$ MEFs.

The *Ink4a/Arf* locus encodes the important tumor suppressors p16^{Ink4a} and p19^{ARF}. This locus is deleted in a wide spectrum of tumors including melanoma, pancreatic adenocarcinoma, glioblastoma, certain leukemias, non-small-cell lung cancer and bladder carcinoma (Lomas *et al.*, 2008; Maitra and Hruban, 2008; Solomon *et al.*, 2008). We have now shown that the expression of p16^{Ink4a} and p19^{ARF} is increased in *Fbxw7*$^{\Delta/\Delta}$ MEFs. This upregulation did not appear to be attributable to activation of Notch signaling, given that it was not recapitulated by forced expression of NICD1 or abolished by disruption of *Rbpj*. Conversely, c-Myc was previously shown to regulate the *Ink4a/Arf* locus by directly associating with E-box elements within the genomic DNA (Guney *et al.*, 2006). c-Myc is a highly labile protein (half-life of ~30 min), with its stability being primarily determined by Fbxw7-mediated ubiquitylation (Welcker *et al.*, 2004; Yada *et al.*, 2004). We found that the expression of p16^{Ink4a} and p19^{ARF} was also increased at the transcriptional level in Fbxw7-deficient MEFs. In addition, overexpression of c-Myc in wild-type MEFs resulted in an increase in the expression of p19^{ARF} (but not in that of p16^{Ink4a}) at both the mRNA and protein levels. Furthermore, the increased expression of p19^{ARF} in *Fbxw7*$^{\Delta/\Delta}$ MEFs was normalized by genetic ablation of c-Myc, consistent with the notion that the accumulation of c-Myc is primarily responsible for the upregulation of p19^{ARF} in these cells. Given that overexpression of c-Myc did not mimic the increased expression of p16^{Ink4a} apparent in Fbxw7-deficient MEFs, p16^{Ink4a} might be regulated by an unknown substrate(s) of the SCF^{Fbxw7} ubiquitin ligase (Figure 7). The results of our study are consistent with the previous observation that c-Myc appeared to have little, if any, effect on p16^{Ink4a} expression in MEFs (Zindy *et al.*, 1998; Drayton *et al.*, 2003).

The expression of p19^{ARF} in MEFs was shown to be regulated at the level of protein stability as well as of transcription. Our observation that the stability of p19^{ARF} is increased in Fbxw7-null MEFs was unexpected, given that the amino-acid sequence of p19^{ARF} does not contain a typical degron sequence for Fbxw7 (CPD, or Cdc4 phosphodegron). Several studies have

revealed functional relations among c-Myc, nucleophosmin (NPM, also known as B23), p19^{ARF} and Fbxw7. c-Myc thus induces p19^{ARF} and *NPM* gene transcription, and both p19^{ARF} and *NPM* interact with and thereby regulate c-Myc (Zeller *et al.*, 2001; Datta *et al.*, 2004; Qi *et al.*, 2004; Li *et al.*, 2008). NPM also binds to p19^{ARF} and protects it from degradation, as revealed by the destabilization of p19^{ARF} apparent in *Npm*$^{-/-}$ MEFs (Colombo *et al.*, 2005). Furthermore, a recent study suggested that NPM is required for the nucleolar localization and stabilization of the γ-isoform of Fbxw7, which results in promotion of c-Myc degradation by Fbxw7 (Bonetti *et al.*, 2008). These lines of evidence suggest that Fbxw7 regulates p19^{ARF} expression at various levels.

We have shown here that Fbxw7 regulates the expression of the CKIs p27^{Kip1} and p57^{Kip2} and the tumor suppressors p16^{Ink4a} and p19^{ARF} in opposite directions through the degradation of NICD1, c-Myc and an unknown substrate(s) in MEFs (Figure 7). The decrease in the expression of p27^{Kip1} and p57^{Kip2} induced by ablation of Fbxw7 may promote cell proliferation, whereas the increase in that of p21^{Cip1}, p16^{Ink4a} and p19^{ARF} may induce growth arrest. The latter effect appears to be predominant in Fbxw7-null MEFs, suggesting that the impact of the upregulation of p21^{Cip1}, p16^{Ink4a} and p19^{ARF} is greater than that of the downregulation of p27^{Kip1} and p57^{Kip2}. Our previous study showed that the cell-cycle arrest in *Fbxw7*$^{\Delta/\Delta}$ MEFs is largely dependent on Notch1 and p53 (Ishikawa *et al.*, 2008), suggesting that p21^{Cip1} might be the one of the most critical regulators for the cell-cycle arrest. However, the increase in the abundance of p21^{Cip1} in *Fbxw7*$^{\Delta/\Delta}$ MEFs was not obvious in the previous study in which aged MEFs (>1 week after gene ablation) were used (Ishikawa *et al.*, 2008), probably because p21^{Cip1} was upregulated in the control cells by senescence that made the difference in p21^{Cip1} expression less pronounced between wild-type and mutant cells. To avoid the background increase of p21^{Cip1}, we analyzed the regulation of CKIs within 1 week after gene ablation in this study, and found that p21^{Cip1} was indeed increased to a greater extent in *Fbxw7*$^{\Delta/\Delta}$ MEFs than that in wild-type cells. We do not exclude the possibility that other targets of p53 such as 14-3-3σ might be involved in the cell-cycle arrest of *Fbxw7*$^{\Delta/\Delta}$ MEFs. To further investigate the role of p21^{Cip1}, generation and characterization of *Fbxw7*$^{\Delta/\Delta}$, *p21*$^{-/-}$ MEFs will be necessary. Collectively, given that *FBXW7* is a potential oncosuppressor gene in various types of human cancer (Nakayama and Nakayama, 2006; Akhoondi *et al.*, 2007; Welcker and Clurman, 2008), these molecular interactions in MEFs may provide insight into the role of Fbxw7 in carcinogenesis in a variety of tissues.

Materials and methods

Cells and viral infection

Fbxw7$^{+/+}$, *Fbxw7*$^{+/F}$ and *Fbxw7*$^{F/F}$ MEFs were prepared at embryonic day 13.5 from embryos generated by mating of *Fbxw7*$^{+/F}$ mice (Onoyama *et al.*, 2007) and were maintained as previously described (Nakayama *et al.*, 1996). *Fbxw7*$^{F/F}$*Rbpj*$^{F/F}$, *Fbxw7*$^{F/F}$*p53*$^{-/-}$ and *Fbxw7*$^{F/F}$*c-Myc*$^{F/F}$ MEFs were prepared from embryos generated by breeding *Fbxw7*$^{+/F}$*Rbpj*$^{F/F}$ mice (Han *et al.*, 2002), *Fbxw7*$^{+/F}$*p53*$^{-/-}$ mice (Taconic, Germantown, NY, USA) or *Fbxw7*$^{+/F}$*c-Myc*$^{F/F}$ mice (de Alboran *et al.*, 2004), respectively. All experiments in this study were performed with nonsenescent MEFs (<2 passages) within 1 week after gene ablation.

Complementary DNAs encoding Cre recombinase or mouse NICD1 were subcloned into the retroviral vectors pMX-puro or pMX-blast (Morita *et al.*, 2000), and that encoding mouse c-Myc was subcloned into the retroviral vector pBabe-puro (Morgenstern and Land, 1990). Plat-E packaging cells were transfected with these vectors with the use of the FuGENE6 reagent (Roche, Indianapolis, IN, USA), and culture supernatants containing recombinant ecotropic retroviruses were harvested. Conditional inactivation of *Fbxw7*, *Rbpj* or *c-Myc* was performed by infection of MEFs harboring the corresponding floxed (F) alleles with a retrovirus encoding Cre recombinase. Proliferating MEFs were incubated with virus-containing culture supernatants in the presence of Polybrene (2 μg/ml) for 12 h. At 24 h after infection, the cells were subjected to selection in medium containing puromycin (10 μg/ml) or blasticidin (2 μg/ml) for 72 h.

For serum deprivation, cells were washed twice with phosphate-buffered saline and cultured for 96 h in Dulbecco's modified Eagle's medium supplemented with 0.05% fetal bovine serum. For analysis of growth rate, we seeded cells in 15 cm culture dishes at a density of 1×10^5 per dish, harvested at the indicated times and counted using a hemocytometer.

RNA interference

For RNAi-mediated depletion of Notch1, 3×10^5 MEFs were transfected with 2 μl of stock Stealth RNAi duplex (20 mM) using Neon Transfection System (Invitrogen, Carlsbad, CA, USA). At 24 h after transfection, the cells were subjected to serum deprivation in Dulbecco's modified Eagle's medium containing 0.1% fetal bovine serum for 60 h. Sequence information for *Notch1* RNAi, 5′-GGTCTGCAACCTGCAG TGTAATAAT-3′. As a control, Stealth RNAi Negative Control Duplexes were used.

Quantitative RT–PCR analysis

Total RNA was isolated from cells and purified using an SV Total RNA Isolation System (Promega, Madison, WI, USA). Complementary DNA was synthesized from the RNA by reverse transcription (RT) with the use of a PrimerScript RT reagent kit (Takara Bio, Shiga, Japan) and was subjected to real-time PCR analysis with a 7000 sequence detection system and the Power SYBR Green dye (Applied Biosystems, Foster City, CA, USA). Data were analyzed according to the $2^{-\Delta\Delta Ct}$ method and were normalized relative to the amount of acidic ribosomal phosphoprotein mRNA. The normalized abundance of target mRNAs was expressed relative to the corresponding value for wild-type or control cells. PCR was performed with the following primers (forward and reverse, respectively): acidic ribosomal phosphoprotein, 5′-GGACCCG AGAAGACCTCCTT-3′ and 5′-GCACATCACTCAGAATTT CAATGG-3′; Fbxw7, 5′-TGCAAAGTCTCAGATTATACC-3′ and 5′-TTTCTCTCTCCAGAGAAGGTTATC-3′; HeyL, 5′-GA CGGCGAGTCTGATGGAC-3′ and 5′-TTCTTCCGGGCTT GCATC-3′; p16^{Ink4a}, 5′-GAACTCTTTCGGTCGTACCC-3′ and 5′-CAGTTCGAATCTGCACCGTAG-3′; p19^{ARF}, 5′-CAT GTTGTTGAGGCTAGAGAGG-3′ and 5′-TGAGCAGAAG AGCTGCTACG-3′; p27^{Kip1}, 5′-AACTAACCCGGGACTTG

GAG-3′ and 5′-CACCTCCTGCCATTCGTATC-3′; p57^{Kip2}, 5′-CACTCTGTACCATGTGCAAGGAGTA-3′ and 5′-TTTC TCTTTTTGTTTTGCACTGAGA-3′; Skp2, 5′-TTAGTCGG GAGAACTTTCCAGGTG-3′ and 5′-AGTCACGTCTGGG TGCAGATTT-3′; c-Myc, 5′-TGAGCCCCTAGTGCTGCA T-3′ and 5′-AGCCCGACTCCGACCTCTT-3′; and Notch1, 5′-CCGTTACATGCAGCAGTTTC-3′ and 5′-AGCCAGGAT CAGTGGAGTTG-3′.

Protein analysis

Whole-cell extracts were subjected to immunoblot analysis as described (Kitagawa *et al*., 1999). Primary antibodies included those to c-Myc (N-262), Cdk4 (C-22) or p16^{Ink4a} (M-156), all of which were obtained from Santa Cruz Biotechnology (Santa Cruz, CA, USA); Notch1 (Cell Signaling, Danvers, MA, USA); p57^{Kip2} (B-5-1-2; Sigma, St Louis, MO, USA); p27^{Kip1}, p21^{Cip1} or Hsp90 (BD Pharmingen, San Diego, CA, USA); p53 (Novocastra, Newcastle, UK) and p19^{ARF} (ab80; Abcam, Cambridge, UK). For analysis of c-Myc or p19^{ARF} stability, cells were exposed to cycloheximide (100 μg/ml) and harvested at the indicated times thereafter.

Flow cytometry

For analysis of cell-cycle profile, cells were incubated with 10 μM bromodeoxyuridine (BrdU; Sigma) for 60 min and then stained with propidium iodide and fluorescein isothiocyanate (FITC)-conjugated antibodies to BrdU (BD Pharmingen). Only cells with a DNA content of 2C or 4C were counted. For detection of apoptosis, MEFs were harvested and stained with FITC-conjugated annexin V and counterstained with propidium iodide (Annexin V-FITC Apoptosis Detection Kit; BD Pharmingen). All analyses were performed with an Epics XL flow cytometer and FlowJo software (Tomy Digital Biology, Tokyo, Japan).

Statistical analysis

Quantitative data are presented as means ± s.d. and were analyzed by Student's *t*-test. A *P*-value of <0.05 was considered statistically significant. All experiments were performed at least three times.

Conflict of interest

The authors declare no conflict of interest.

Acknowledgements

We thank T Honjo for providing *Rbpj*$^{F/F}$ mice; R Tsunematsu for an NICD1 plasmid; T Kitamura for pMX-puro and Plat-E cells; T Senga, Y Ono and N Kobayashi for technical assistance; and N Yanagihara, N Ishida and other laboratory members for helpful discussion and Y Akaida for help in preparation of the paper. This study was supported in part by a Grant-in-Aid and the Network Medicine Global COE Program from the Ministry of Education, Culture, Sports, Science and Technology of Japan.

References

Akhoondi S, Sun D, von der Lehr N, Apostolidou S, Klotz K, Maljukova A *et al.* (2007). FBXW7/hCDC4 is a general tumor suppressor in human cancer. *Cancer Res* **67**: 9006–9012.

Artavanis-Tsakonas S, Rand MD, Lake RJ. (1999). Notch signaling: cell fate control and signal integration in development. *Science* **284**: 770–776.

Besson A, Hwang HC, Cicero S, Donovan SL, Gurian-West M, Johnson D *et al.* (2007). Discovery of an oncogenic activity in p27^{Kip1} that causes stem cell expansion and a multiple tumor phenotype. *Genes Dev* **21**: 1731–1746.

Bonetti P, Davoli T, Sironi C, Amati B, Pelicci PG, Colombo E. (2008). Nucleophosmin and its AML-associated mutant regulate c-Myc turnover through Fbw7γ. *J Cell Biol* **182**: 19–26.

Coats S, Flanagan WM, Nourse J, Roberts JM. (1996). Requirement of p27^{Kip1} for restriction point control of the fibroblast cell cycle. *Science* **272**: 877–880.

Colombo E, Bonetti P, Lazzerini Denchi E, Martinelli P, Zamponi R, Marine JC *et al* (2005). Nucleophosmin is required for DNA integrity and p19^{Arf} protein stability. *Mol Cell Biol* **25**: 8874–8886.

Datta A, Nag A, Pan W, Hay N, Gartel AL, Colamonici O *et al.* (2004). Myc-ARF (alternate reading frame) interaction inhibits the functions of Myc. *J Biol Chem* **279**: 36698–36707.

de Alboran IM, Baena E, Martinez AC. (2004). c-Myc-deficient B lymphocytes are resistant to spontaneous and induced cell death. *Cell Death Differ* **11**: 61–68.

Drayton S, Rowe J, Jones R, Vatcheva R, Cuthbert-Heavens D, Marshall J *et al.* (2003). Tumor suppressor p16^{INK4a} determines sensitivity of human cells to transformation by cooperating cellular oncogenes. *Cancer Cell* **4**: 301–310.

Georgia S, Soliz R, Li M, Zhang P, Bhushan A. (2006). p57 and Hes1 coordinate cell cycle exit with self-renewal of pancreatic progenitors. *Dev Biol* **298**: 22–31.

Guney I, Wu S, Sedivy JM. (2006). Reduced c-Myc signaling triggers telomere-independent senescence by regulating Bmi-1 and p16^{INK4a}. *Proc Natl Acad Sci USA* **103**: 3645–3650.

Han H, Tanigaki K, Yamamoto N, Kuroda K, Yoshimoto M, Nakahata T *et al.* (2002). Inducible gene knockout of transcription factor recombination signal binding protein-J reveals its essential role in T versus B lineage decision. *Int Immunol* **14**: 637–645.

Hubbard EJ, Wu G, Kitajewski J, Greenwald I. (1997). sel-10, a negative regulator of lin-12 activity in *Caenorhabditis elegans*, encodes a member of the CDC4 family of proteins. *Genes Dev* **11**: 3182–3193.

Ishikawa Y, Onoyama I, Nakayama KI, Nakayama K. (2008). Notch-dependent cell cycle arrest and apoptosis in mouse embryonic fibroblasts lacking Fbxw7. *Oncogene* **27**: 6164–6174.

Jia J, Lin M, Zhang L, York JP, Zhang P. (2007). The Notch signaling pathway controls the size of the ocular lens by directly suppressing p57^{Kip2} expression. *Mol Cell Biol* **27**: 7236–7247.

Kamura T, Hara T, Kotoshiba S, Yada M, Ishida N, Imaki H *et al.* (2003). Degradation of p57^{Kip2} mediated by SCF^{Skp2}-dependent ubiquitylation. *Proc Natl Acad Sci USA* **100**: 10231–10236.

Kato H, Sakai T, Tamura K, Minoguchi S, Shirayoshi Y, Hamada Y *et al.* (1996). Functional conservation of mouse Notch receptor family members. *FEBS Lett* **395**: 221–224.

Kitagawa M, Hatakeyama S, Shirane M, Matsumoto M, Ishida N, Hattori K *et al.* (1999). An F-box protein, FWD1, mediates ubiquitin-dependent proteolysis of β-catenin. *EMBO J* **18**: 2401–2410.

Knuutila S, Aalto Y, Autio K, Bjorkqvist AM, El-Rifai W, Hemmer S *et al.* (1999). DNA copy number losses in human neoplasms. *Am J Pathol* **155**: 683–694.

Koepp DM, Schaefer LK, Ye X, Keyomarsi K, Chu C, Harper JW *et al.* (2001). Phosphorylation-dependent ubiquitination of cyclin E by the SCF^{Fbw7} ubiquitin ligase. *Science* **294**: 173–177.

Li Z, Boone D, Hann SR. (2008). Nucleophosmin interacts directly with c-Myc and controls c-Myc-induced hyperproliferation and transformation. *Proc Natl Acad Sci USA* **105**: 18794–18799.

Lomas J, Martin-Duque P, Pons M, Quintanilla M. (2008). The genetics of malignant melanoma. *Front Biosci* **13**: 5071–5093.

Maitra A, Hruban RH. (2008). Pancreatic cancer. *Annu Rev Pathol* **3**: 157–188.

Mao JH, Perez-Losada J, Wu D, Delrosario R, Tsunematsu R, Nakayama KI *et al.* (2004). Fbxw7/Cdc4 is a p53-dependent, haploinsufficient tumour suppressor gene. *Nature* **432**: 775–779.

Matsuoka S, Oike Y, Onoyama I, Iwama A, Arai F, Takubo K *et al.* (2008). Fbxw7 acts as a critical fail-safe against premature loss of hematopoietic stem cells and development of T-ALL. *Genes Dev* **22**: 986–991.

Moberg KH, Bell DW, Wahrer DC, Haber DA, Hariharan IK. (2001). Archipelago regulates Cyclin E levels in Drosophila and is mutated in human cancer cell lines. *Nature* **413**: 311–316.

Morgenstern JP, Land H. (1990). Advanced mammalian gene transfer: high titre retroviral vectors with multiple drug selection markers and a complementary helper-free packaging cell line. *Nucleic Acids Res* **18**: 3587–3596.

Morita S, Kojima T, Kitamura T. (2000). Plat-E: an efficient and stable system for transient packaging of retroviruses. *Gene Therapy* **7**: 1063–1066.

Murata K, Hattori M, Hirai N, Shinozuka Y, Hirata H, Kageyama R *et al.* (2005). Hes1 directly controls cell proliferation through the transcriptional repression of p27^{Kip1}. *Mol Cell Biol* **25**: 4262–4271.

Nakayama K, Ishida N, Shirane M, Inomata A, Inoue T, Shishido N *et al.* (1996). Mice lacking p27^{Kip1} display increased body size, multiple organ hyperplasia, retinal dysplasia, and pituitary tumors. *Cell* **85**: 707–720.

Nakayama KI, Nakayama K. (2006). Ubiquitin ligases: cell-cycle control and cancer. *Nat Rev Cancer* **6**: 369–381.

Nateri AS, Riera-Sans L, Da Costa C, Behrens A. (2004). The ubiquitin ligase SCF^{Fbw7} antagonizes apoptotic JNK signaling. *Science* **303**: 1374–1378.

Onoyama I, Nakayama KI. (2008). Fbxw7 in cell cycle exit and stem cell maintenance: insight from gene-targeted mice. *Cell Cycle* **7**: 3307–3313.

Onoyama I, Tsunematsu R, Matsumoto A, Kimura T, de Alboran IM, Nakayama K *et al.* (2007). Conditional inactivation of Fbxw7 impairs cell-cycle exit during T cell differentiation and results in lymphomatogenesis. *J Exp Med* **204**: 2875–2888.

Qi Y, Gregory MA, Li Z, Brousal JP, West K, Hann SR. (2004). p19^{ARF} directly and differentially controls the functions of c-Myc independently of p53. *Nature* **431**: 712–717.

Riccio O, van Gijn ME, Bezdek AC, Pellegrinet L, van Es JH, Zimber-Strobl U *et al.* (2008). Loss of intestinal crypt progenitor cells owing to inactivation of both Notch1 and Notch2 is accompanied by derepression of CDK inhibitors p27^{Kip1} and p57^{Kip2}. *EMBO Rep* **9**: 377–383.

Sarmento LM, Huang H, Limon A, Gordon W, Fernandes J, Tavares MJ *et al* (2005). Notch1 modulates timing of G1-S progression by inducing SKP2 transcription and p27^{Kip1} degradation. *J Exp Med* **202**: 157–168.

Solomon DA, Kim JS, Jean W, Waldman T. (2008). Conspirators in a capital crime: co-deletion of p18^{INK4c} and p16^{INK4a}/p14^{ARF}/p15^{INK4b} in glioblastoma multiforme. *Cancer Res* **68**: 8657–8660.

Strohmaier H, Spruck CH, Kaiser P, Won KA, Sangfelt O, Reed SI. (2001). Human F-box protein hCdc4 targets cyclin E for proteolysis and is mutated in a breast cancer cell line. *Nature* **413**: 316–322.

Sundaram M, Greenwald I. (1993). Suppressors of a *lin-12* hypomorph define genes that interact with both *lin-12* and *glp-1* in *Caenorhabditis elegans*. *Genetics* **135**: 765–783.

Tetzlaff MT, Yu W, Li M, Zhang P, Finegold M, Mahon K *et al.* (2004). Defective cardiovascular development and elevated cyclin E and Notch proteins in mice lacking the Fbw7 F-box protein. *Proc Natl Acad Sci USA* **101**: 3338–3345.

Thompson BJ, Jankovic V, Gao J, Buonamici S, Vest A, Lee JM *et al.* (2008). Control of hematopoietic stem cell quiescence by the E3 ubiquitin ligase Fbw7. *J Exp Med* **205**: 1395–1408.

Tsunematsu R, Nakayama K, Oike Y, Nishiyama M, Ishida N, Hatakeyama S *et al.* (2004). Mouse Fbw7/Sel-10/Cdc4 is required for notch degradation during vascular development. *J Biol Chem* **279**: 9417–9423.

Urano T, Yashiroda H, Muraoka M, Tanaka K, Hosoi T, Inoue S *et al.* (1999). p57^{Kip2} is degraded through the proteasome in osteoblasts stimulated to proliferation by transforming growth factor beta1. *J Biol Chem* **274**: 12197–12200.

Vernon AE, Movassagh M, Horan I, Wise H, Ohnuma S, Philpott A. (2006). Notch targets the Cdk inhibitor Xic1 to regulate differentiation but not the cell cycle in neurons. *EMBO Rep* **7**: 643–648.

Welcker M, Clurman BE. (2008). FBW7 ubiquitin ligase: a tumour suppressor at the crossroads of cell division, growth and differentiation. *Nat Rev Cancer* **8**: 83–93.

Welcker M, Orian A, Grim JE, Eisenman RN, Clurman BE. (2004). A nucleolar isoform of the Fbw7 ubiquitin ligase regulates c-Myc and cell size. *Curr Biol* **14**: 1852–1857.

Yada M, Hatakeyama S, Kamura T, Nishiyama M, Tsunematsu R, Imaki H *et al.* (2004). Phosphorylation-dependent degradation of c-Myc is mediated by the F-box protein Fbw7. *EMBO J* **23**: 2116–2125.

Zeller KI, Haggerty TJ, Barrett JF, Guo Q, Wonsey DR, Dang CV. (2001). Characterization of nucleophosmin (B23) as a Myc target by scanning chromatin immunoprecipitation. *J Biol Chem* **276**: 48285–48291.

Zindy F, Eischen CM, Randle DH, Kamijo T, Cleveland JL, Sherr CJ *et al.* (1998). Myc signaling via the ARF tumor suppressor regulates p53-dependent apoptosis and immortalization. *Genes Dev* **12**: 2424–2433.

KDM7 is a dual demethylase for histone H3 Lys 9 and Lys 27 and functions in brain development

Yu-ichi Tsukada, Tohru Ishitani and Keiichi I. Nakayama

Genes Dev. 2010 24: 432-437
Access the most recent version at doi:10.1101/gad.1864410

RESEARCH COMMUNICATION

KDM7 is a dual demethylase for histone H3 Lys 9 and Lys 27 and functions in brain development

Yu-ichi Tsukada,[1,2,3] Tohru Ishitani,[4] and Keiichi I. Nakayama[1,2,5]

[1]Division of Cell Biology, Medical Institute of Bioregulation, Kyushu University, Higashi-ku, Fukuoka 812-8582, Japan; [2]CREST, Japan Science and Technology Agency (JST), Kawaguchi, Saitama 332-0012, Japan; [3]PRESTO, Japan Science and Technology Agency (JST), Kawaguchi, Saitama 332-0012, Japan; [4]Division of Cell Regulation Systems, Medical Institute of Bioregulation, Kyushu University, Higashi-ku, Fukuoka 812-8582, Japan

Methylation of histone H3 Lys 9 and Lys 27 (H3K9 and H3K27) is associated with transcriptional silencing. Here we show that KDM7, a JmjC domain-containing protein, catalyzes demethylation of both mono- or dimethylated H3K9 and H3K27. Inhibition of KDM7 orthologs in zebrafish resulted in developmental brain defects. KDM7 interacts with the follistatin gene locus, and KDM7 depletion in mammalian neuronal cells suppressed follistatin gene transcription in association with increased levels of dimethylated H3K9 and H3K27. Our findings identify KDM7 as a dual demethylase for H3K9 and H3K27 that functions as an eraser of silencing marks on chromatin during brain development.

Supplemental material is available at http://www.genesdev.org.

Received September 16, 2009; revised version accepted December 31, 2009.

Histone methylation status defines the epigenetic program of a cell by determining chromatin structure and thereby regulating DNA-dependent processes such as transcription (Strahl and Allis 2000; Lachner et al. 2003; Margueron et al. 2005; Martin and Zhang 2005). Histone methylation has also been linked to regulation of neuronal function (Iwase et al. 2007). The recent discovery of histone demethylases revealed that histone methylation is a more dynamic process than previously recognized, and that most identified demethylases show a strict substrate specificity limited to a single methylation site (Bannister et al. 2002; Shi et al. 2004; Klose et al. 2006a; Tsukada et al. 2006; Shi and Whetstine 2007; Cloos et al. 2008; Lan et al. 2008). A number of histone demethylases contain a JmjC domain, and a subfamily of JmjC domain-containing proteins (comprising KIAA1718, PHF8, and PHF2) is evolutionarily conserved from *Caenorhabditis elegans* to humans and is characterized by the presence of a PHD-type zinc finger motif in addition to the JmjC domain (Supplemental Fig. S1A). Whereas the human genes for PHF8 and PHF2 are associated with X-linked mental retardation and hereditary sensory neuropathy type I, respectively (Hasenpusch-Theil et al. 1999; Laumonnier et al. 2005; Abidi et al. 2007; Koivisto et al. 2007), little is known about KIAA1718. Bioinformatic analysis of the JmjC domains of KIAA1718, PHF8, and PHF2 indicated that predicted Fe(II)- and α-ketoglutarate (α-KG)-binding sites are conserved, with the exception of the former in PHF2, and that they share extensive similarity with the JmjC domain of JHDM1/KDM2 (Supplemental Fig. S1B). Conservation of residues within the putative cofactor-binding sites of KIAA1718 suggested that this protein might possess histone demethylase activity, and therefore might also contribute to transcriptional regulation of genes in the nervous system.

[*Keywords*: Demethylase; JmjC; methylation; histone; chromatin; epigenetics]
[5]Corresponding author.
E-MAIL nakayak1@bioreg.kyushu-u.ac.jp; FAX 81-92-642-6819.
Article is online at http://www.genesdev.org/cgi/doi/10.1101/gad.1864410.

Results and Discussion

KIAA1718 possesses histone demethylase activity

To examine whether KIAA1718 indeed possesses histone demethylase activity, we generated the mouse protein tagged with the Flag epitope at its C terminus in insect cells (Fig. 1A), and incubated the recombinant protein with histone substrates labeled with ^{3}H at various characterized methyl-lysine or methyl-arginine sites by corresponding histone methyltransferases (HMTs). Histone demethylase activity was monitored by measurement of the release of the labeled demethylation product, formaldehyde. Substantial release of labeled formaldehyde was observed in the reaction mixture containing histone H3 labeled on Lys 9 (H3K9) by G9a, but not in those containing histone substrates modified by other HMTs (Fig. 1B). Consistent with the notion that the observed enzymatic activity was intrinsic to KIAA1718, formaldehyde release from G9a-labeled H3 was dependent on KIAA1718 concentration (Fig. 1C). To ascertain whether the demethylation mediated by KIAA1718 is oxidative in nature, with Fe(II) and α-KG as cofactors, we examined whether the enzymatic activity of KIAA1718 is dependent on these cofactors. The release of formaldehyde mediated by KIAA1718 was indeed found to require both Fe(II) and α-KG (Fig. 1D). Ascorbate was also required for the enzymatic activity, presumably as a result of its ability to regenerate Fe(II) from Fe(III). To verify further that the observed enzymatic activity is attributable to a genuine demethylase, we generated recombinant forms of KIAA1718 that either lack the JmjC or PHD domains or contain a mutation (H282A) in the Fe(II)-binding site in insect cells (Fig. 1E). Analysis of similar amounts of the mutant proteins for histone demethylase activity revealed that deletion of the JmjC domain or mutation of His^{282} abolished the activity of KIAA1718, whereas the PHD domain appeared to be dispensable for such activity (Fig. 1E,F). Together, these results showed that KIAA1718 is a histone demethylase capable of removing methyl groups from H3K9. Given that histone demethylase activity is the first function attributed to KIAA1718, we named this protein KDM7 on the basis of the previously described nomenclature (Allis et al. 2007).

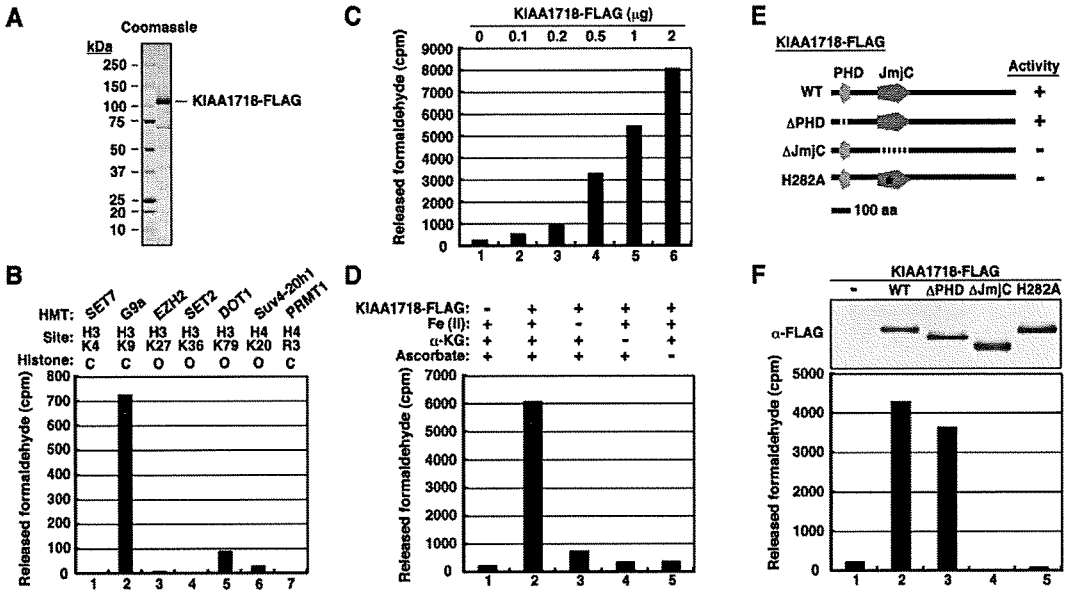

Figure 1. KIAA1718 is a histone demethylase that targets H3K9. (*A*, *right* lane) SDS–polyacrylamide gel electrophoresis with Coomassie blue staining of a C-terminally Flag-tagged recombinant KIAA1718 protein. Molecular size standards are shown in the *left* lane. (*B*) Histone demethylase activity of purified KIAA1718-Flag with various methylated histone substrates. The HMTs used to generate the various substrates and their sites of methylation are indicated. The methylated substrates were generated with the indicated forms of histone ([C] core histone octamer; [O] oligonucleosome) on the basis of the substrate preference of each HMT. The presented counts have been corrected for control counts. (*C*) Histone demethylase activity of the indicated amounts of KIAA1718-Flag. (*D*) Effects of removal of Fe(II), α-KG, or ascorbate from the reaction mixture on the histone demethylase activity of KIAA1718-Flag with G9a-methylated histone substrate. (*E*) Schematic representation of wild-type (WT) and mutant forms of KIAA1718 showing whether they are active (+) or inactive (−) as H3K9 demethylases. (*F*, *bottom* panel) Demethylase activity of purified wild-type or mutant forms of KIAA1718-Flag with G9a-methylated histone substrate. (*Top* panel) The similar amounts of KIAA1718-Flag proteins used in the demethylase assay are revealed by immunoblot analysis with antibodies to Flag (α-Flag).

KDM7 is a dual demethylase for dimethylated and monomethylated H3K9 (H3K9me2/me1) and H3K27me2/me1

To define the substrate and modification state specificity of KDM7, we included core histones as substrates in demethylation reaction mixtures and examined the modification status of individual methylation sites by immunoblot analysis with a series of methylation-specific antibodies. Wild-type KDM7 mediated a marked decrease in the methylation level of both H3K9me2 and H3K27me2, without affecting that of other histone methylation sites (Fig. 2A; Supplemental Fig. S2A). In addition, KDM7 efficiently removed methyl groups from H3K9me2 and H3K27me2 in core histones, but not from those in mono- or oligonucleosomes (Supplemental Fig. S2B,C). These results suggested that KDM7 prefers core histones rather than mono- or oligonucleosomes as substrates, and explain why demethylase activity was not detected by the radioactive formaldehyde release assay with nucleosomal histones methylated by the HMT EZH2 (Fig. 1B). They also suggested that the low level of reactivity apparent in the formaldehyde release assay with oligonucleosomes modified by DOT1 or Suv4-20h1 as substrates does not reflect demethylase activity of KDM7. To refine further the specificity of KDM7, we used methylated peptides as substrates in demethylation reactions and analyzed the removal of methyl groups from the peptides by mass spectrometry. This assay showed that KDM7 removed methyl groups from both H3K9me2 and H3K27me2 (Fig. 2B,C), eliminating the possibility of cross-reaction of antibodies between methylated H3K9 and H3K27 in the immunoblot analysis. KDM7 also demethylated both H3K9me1 and H3K27me1 (Fig. 2B,C), activity that was not apparent by immunoblot analysis (Fig. 2A), probably because demethylation by KDM7 is not highly processive, so that a reduction in the level of monomethylation is masked by production of monomethylated histone from dimethylated histone in a reaction with core histones that contain all three states of methylation, as compared with peptides containing a single monomethylation state. No demethylation was detected with trimethylated H3K9 (H3K9me3) or H3K27me3 peptides. A low level of demethylation activity was also apparent with an H3K36me2 peptide, but no demethylation of H3K36me1 or H3K36me3 was detected (Fig. 2D). The decrease in mass corresponding to a methyl group was not detected in reaction mixtures containing other methylated histone peptides (Supplemental Fig. S3). Together, these data suggested that KDM7 is an authentic histone demethylase with the ability to mediate the direct removal of methyl groups from H3K9me2/me1 and H3K27me2/me1.

Zebrafish KDM7 orthologs possess histone demethylase activity for H3K9/K27 and are expressed predominantly in the brain

To explore the biological function of KDM7 in vivo, we characterized the KDM7 orthologs in zebrafish—LOC321248 and LOC558416, hereafter designated drKDM7a and drKDM7b, respectively (Supplemental Fig. S1A)—both of which were also found to manifest histone demethylase activity toward H3K9me2 and

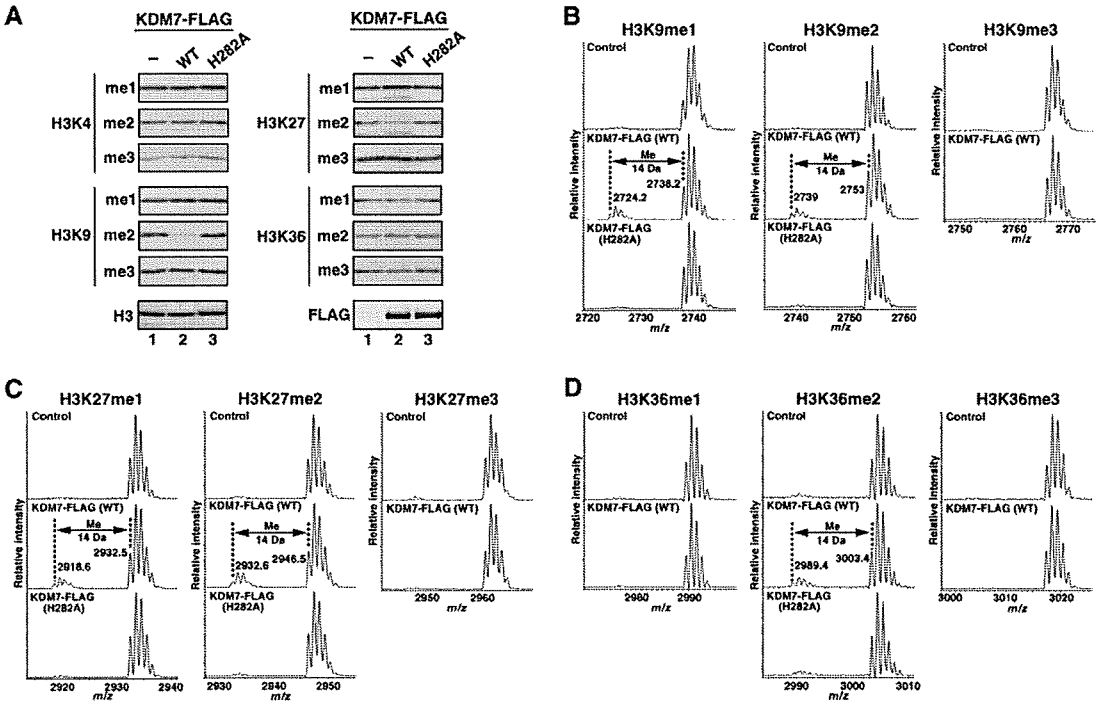

Figure 2. KDM7 is a histone demethylase specific for dimethylated or monomethylated H3K9 or H3K27. (*A*) Calf thymus core histones were incubated in the absence or presence of 5 μg of wild-type or H282A mutant forms of KDM7-Flag, after which histone demethylation was evaluated by immunoblot analysis with antibodies to specific modified histones, as indicated on the *left*. (*B–D*) Mass spectrometric analysis of the demethylase activity of 4 μg of wild-type or H282A mutant forms of KDM7-Flag with methylated H3K9, H3K27, or H3K36 peptide substrates. Numbers represent the masses of the peptide substrates and products.

H3K27me2 in core histones (Supplemental Fig. S4A). We first examined the expression patterns of *kdm7a* and *kdm7b* during development by in situ hybridization. Transcripts corresponding to *kdm7a* and *kdm7b* were detected as early as the post-somitogenesis stage at 24 h post-fertilization (hpf) in the brain and tail bud (Fig. 3A,B), whereas no signals were observed in embryos at 6 or 12 hpf (data not shown). The expression of both *kdm7* genes became prominent in the tectum, hindbrain, fin bud, and gill at 48 hpf (Fig. 3A,B). Corresponding sense probes did not yield any signals at these various stages of development (Supplemental Fig. S4B), indicating that the signals attributed to *kdm7* transcripts were specific.

Zebrafish KDM7 orthologs are required for tectum development

Given that both *kdm7* genes are expressed predominantly in the brain, we examined whether drKDM7 might function in brain development. To examine this possibility, we inhibited the function of drKDM7 with the use of two splicing-blocking antisense morpholino oligonucleotides (MOs) that independently target *kdm7a* or *kdm7b*. We also studied the stable transgenic line Tg(*HuC:Kaede*), which expresses the fluorescent protein Kaede in neurons under the control of the vertebrate neuron-specific promoter of the *HuC* gene, in order to visualize neurons (Sato et al. 2006). The level of mature mRNAs derived from the two *kdm7* genes was reduced specifically in embryos injected with the corresponding MO, but not in those injected with a control MO (Supplemental Fig. S5A). At 48 hpf, embryos that had been subjected to simultaneous injection of both *kdm7* MOs at the one-cell stage manifested a curly tail and marked decrease in size of the tectum (Fig. 3C,D), consistent with the observed expression of *kdm7* in the brain and tail bud. Importantly, the reduction in tectum size was accompanied by the loss of neurons from this region, although neurons in the spinal cord and other regions of the brain were unaffected (Fig. 3D; Supplemental Fig. S5B,C). In contrast, injection of MOs specific for each *kdm7* gene alone elicited only marginal effects compared with those of the control MO, a finding likely attributable to functional redundancy of the two *kdm7* genes. The persistence at 72 hpf of the phenotypes of the embryos injected with both *Kdm7* MOs eliminates the possibility that they were attributable to developmental delay (Fig. 3C; Supplemental Fig. S5B,C). Embryos that had been subjected to simultaneous injection of another set of MOs that independently target *kdm7a* and *kdm7b* also manifested phenotypes (Supplemental Fig. S6) similar to those observed with the original set (Fig. 3C,D), suggesting that the phenotypes were the specific consequence of depletion of *kdm7* transcripts. Coinjection of a validated MO for p53 (Robu et al. 2007) with either of the two independent sets of MOs for *kdm7* did not affect the phenotypes induced by MO-mediated depletion of *kdm7* transcripts (Supplemental Fig. S7), eliminating the possibility that the phenotypes were the result of p53 activation. Given that the phenotypes were not attributable to cell death (Supplemental Fig. S8), drKDM7 might regulate the proliferation or differentiation of neurons. On

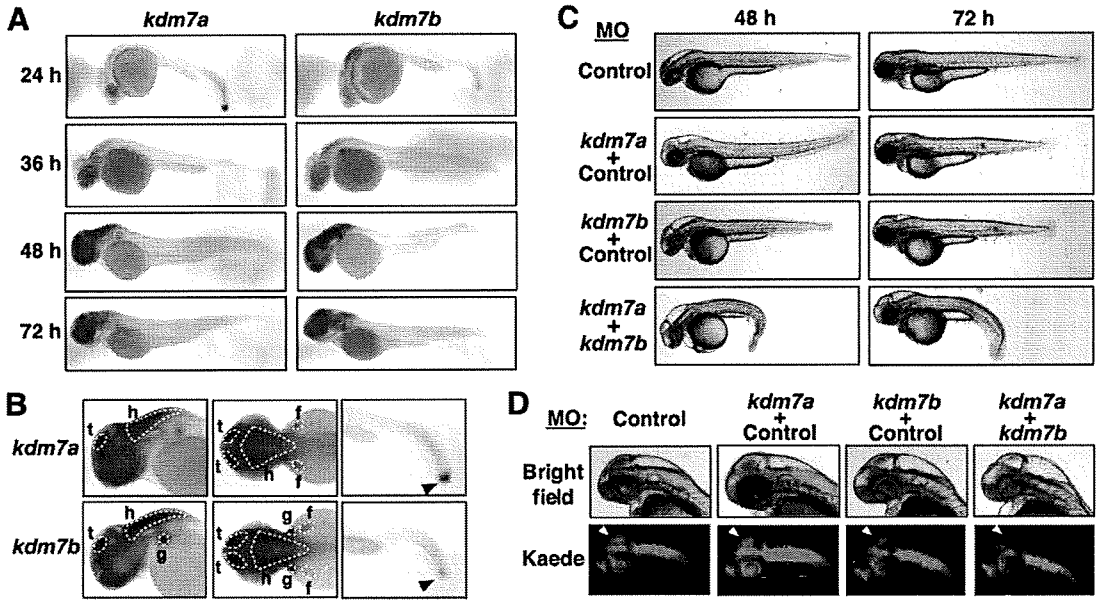

Figure 3. Zebrafish *kdm7* genes are expressed predominantly in brain and are required for tectum development. (*A*) In situ hybridization of whole-mount zebrafish embryos at the indicated stages (hpf) with antisense *kdm7a* or *kdm7b* RNA probes. (*B*) In situ hybridization of whole-mount embryos at 48 hpf (*left* and *middle* panels) or 24 hpf (*right* panels) with antisense *kdm7a* or *kdm7b* RNA probes. Lowercase letters indicate the tectum (t), hindbrain (h), fin bud (f), and gill (g). Arrowheads indicate the tail bud. (*C*) The Tg(*HuC:Kaede*) embryos were injected at the one-cell stage with antisense MOs for *kdm7a* (5 ng) or *kdm7b* (5 ng) or with a control MO (5 or 10 ng for a total of 10 ng of MO) in the indicated combinations. The morphology of the embryos at the indicated times (hpf) was examined by bright-field microscopy. (*D*) Morphology of the head region of embryos at 48 hpf that were injected with MOs as in *C*. (*Bottom* panels) Neurons expressing Kaede under the control of the HuC gene promoter were visualized by fluorescence microscopy. Arrowheads indicate the tectum or presumptive tectal region. Bright-field images are shown in the *top* panels.

the other hand, ectopic overexpression of a fragment of drKDM7a comprising amino acids 1–480 (which manifested demethylase activity similar to that of the full-length protein) achieved by mRNA injection at the one-cell stage resulted in severe developmental defects in zebrafish embryos (Supplemental Fig. S9), suggesting that spatially and temporally regulated expression of drKDM7 is necessary for proper development. Together, these results thus indicated that KDM7 plays an important role in brain development.

KDM7 directly regulates transcription and H3K9me2 and H3K27me2 levels of the follistatin gene

Quantitative RT–PCR analysis revealed that *Kdm7* mRNA was more abundant specifically in the cerebrum and cerebellum than in other mouse tissues, although low levels of *Kdm7* expression were apparent in a wide spectrum of tissues in the mouse (Supplemental Fig. S10A). To investigate the molecular basis for the abnormal brain development in zebrafish embryos depleted of drKDM7, as well as the function of KDM7 in neurons, we examined the effect of KDM7 depletion on the mRNA profile of the mouse neuroblastoma cell line Neuro2A, in which the abundance of KDM7 was found to be greater than that in other cell lines originating from various tissues (Supplemental Fig. S10B). To this end, we stably transfected Neuro2A cells with vectors for two shRNAs—KD1 and KD2—that target two different regions of mouse *Kdm7* mRNA. Quantitative RT–PCR and immunoblot analyses revealed that the amounts of *Kdm7* mRNA and KDM7 protein were markedly decreased in cells transfected with either of these vectors compared with those in parental cells or in cells transfected with a vector for a control shRNA (Fig. 4A,B). Microarray analysis of mRNAs in control cells and in those depleted of KDM7 resulted in the identification of genes whose expression was affected by KDM7 depletion (Supplemental Fig. S10C). One of these genes whose expression was markedly decreased by loss of KDM7 was that for follistatin, on which we initially focused, given that follistatin functions as an endogenous inhibitor of members of the transforming growth factor (TGF)-β superfamily, including activin, which plays an important role in brain development (Hemmati-Brivanlou et al. 1994; Lin et al. 2003; Zhu et al. 2008). We confirmed by quantitative RT–PCR analysis that the abundance of follistatin mRNA was decreased in Neuro2A cells depleted of KDM7 (Fig. 4C). Consistent with the results obtained with Neuro2A cells, depletion of KDM7 by RNAi in primary cultured mouse neurons also resulted in down-regulation of follistatin mRNA (Fig. 4D).

To determine whether the follistatin gene is a direct target of KDM7, we performed a series of chromatin immunoprecipitation (ChIP) experiments to examine its promoter and coding regions in Neuro2A cells (Fig. 4E). This analysis revealed the association of KDM7 with the follistatin gene, predominantly around the transcription start site (Fig. 4F). To investigate the consequences of this association, we analyzed H3K9me2 and H3K27me2 levels in the promoter and coding regions of the gene. Depletion of KDM7 resulted in an increase in both H3K9me2 and H3K27me2 levels around the transcription start site of the gene that appeared to correlate

with KDM7 occupancy (Fig. 4G). Depletion of KDM7 by RNAi in Neuro2A cells did not markedly affect H3K9me3 levels of the follistatin gene (Supplemental Fig. S11A). In contrast, depletion of KDM7 paradoxically increased H3K27me3 levels in the entire region of the gene (Supplemental Fig. S11B), although KDM7 showed no activity toward H3K27me3 in vitro. Given that the regions in which H3K27me3 levels were increased did not correlate with KDM7 occupancy, the observed changes in H3K27me3 levels were most likely an indirect effect of KDM7 depletion. These results suggested that the follistatin gene is a direct target of KDM7-mediated transcriptional activation.

We thus examined whether the zebrafish follistatin gene is dysregulated in *kdm7* morphants with the use of in situ hybridization. Whereas control morphants showed expression of the follistatin gene in an anterior edge region of the tectum at 48 hpf, *kdm7* morphants manifested a substantial decrease in such expression (Fig. 4H). The down-regulation of follistatin gene expression in this particular region was sustained at 60 and 72 hpf (Supplemental Fig. S12A). The corresponding sense probe did not yield any signals at the corresponding stages (Supplemental Fig. S12B). These results thus suggested that KDM7 is recruited to specific regions of the genome, and there functions as an H3K9 and H3K27 demethylase in vivo. To investigate whether follistatin contributes to brain development in zebrafish, we inhibited the function of follistatin with the use of two independent MOs that target the follistatin gene. At 48 hpf, embryos that had been injected with either *follistatin* MO at the one-cell stage manifested a loss of neurons from the tectum region, although neurons in the spinal cord and other regions of the brain were unaffected (Supplemental Fig. S13). Coinjection of the validated MO for p53 did not affect this phenotype (Fig. 4I; Supplemental Fig. S13C). Together, these results indicated that KDM7 contributes to brain development at least in part through regulation of follistatin gene expression.

Methylation of H3K9 and H3K27 is linked to formation of tightly packed chromatin (heterochromatin) and transcriptional silencing (Martin and Zhang 2005). We showed here that KDM7 is a histone demethylase that catalyzes demethylation at both H3K9 and H3K27. Among the JmjC domain-containing histone demethylases, only JHDM3/JMJD2 has been shown to act as a dual demethylase, targeting both H3K9 and H3K36 and functioning as a transcriptional repressor of the ASCL2 gene, although the consequence of simultaneous methylation of these sites remains unclear (Klose et al. 2006b; Whetstine et al. 2006). We therefore propose that KDM7 functions as an eraser of silencing marks on chromatin to unlock gene silencing. Consistent with this notion, we found that removal of methyl groups from H3K9 and H3K27 by KDM7 is associated with transcriptional activation of the follistatin gene. KDM7 belongs to the subfamily of JmjC domain-containing proteins composed of PHF2 and PHF8 in addition to KDM7. The expression of *Phf2* is concentrated in the embryonic neural tube and

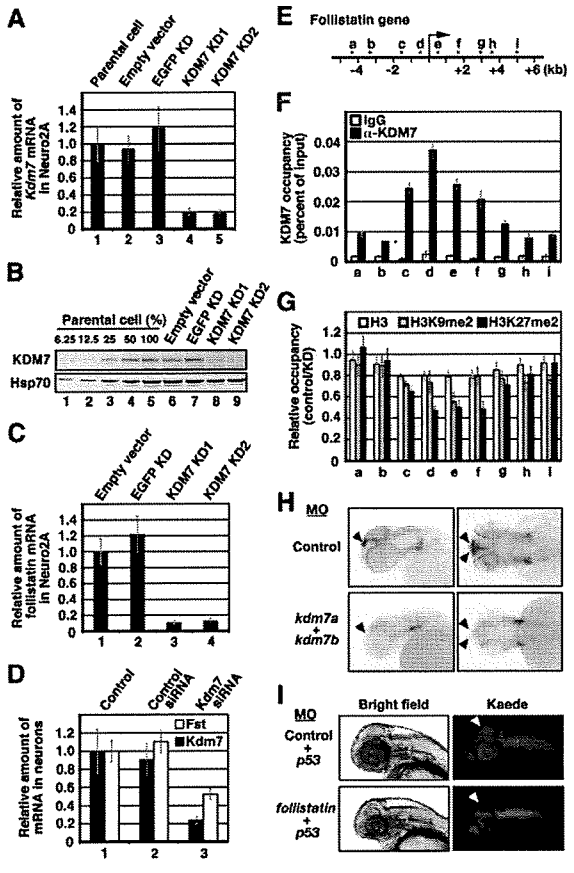

Figure 4. KDM7 directly regulates transcription and both H3K9me2 and H3K27me2 levels of the mouse follistatin gene. (*A*) Quantitative RT–PCR analysis of *Kdm7* mRNA in Neuro2A cell lines stably transfected with vectors for one of two KDM7 shRNAs (KD1 or KD2), with a vector for a control (EGFP) shRNA, or with the empty vector. The amount of *Kdm7* mRNA was normalized by that of *Gapdh* mRNA, and the normalized values are presented relative to that for the parental cells. Data are means ± SD. (*B*) Immunoblot analysis of KDM7 and Hsp70 (loading control) in the cell lines described in *A*. (*C*) Quantitative RT–PCR analysis of follistatin mRNA in the cell lines described in *A*. The amount of follistatin mRNA was normalized by that of *Gapdh* mRNA, and the normalized values are presented relative to that for the cells transfected with the empty vector. Data are means ± SD. (*D*) Quantitative RT–PCR analysis of *Kdm7* and follistatin (*Fst*) mRNAs in primary cultured mouse neurons treated with control or *Kdm7* siRNAs. The amounts of *Kdm7* and follistatin mRNAs were normalized by that of *Gapdh* mRNA, and the normalized values are presented relative to that for control cells. Data are means ± SD. (*E*) Schematic representation of the mouse follistatin genomic locus. The region from a to i was analyzed by ChIP experiments. The transcription start site is indicated by the arrow. (*F*,*G*) ChIP analysis of the relative occupancy of the sites in the follistatin genomic region indicated in *E* with KMD7 (*F*), as well as with H3 (white bars), H3K9me2 (gray bars), and H3K27me2 (black bars) (*G*). The analysis was performed with cells stably transfected with the vector for EGFP shRNA (control) and with cells stably expressing the KD1 shRNA for KDM7 (KD), and the results are presented as the percent of input for control cells (*F*) or the control/KD ratio (*G*). All data are means ± SD. (*H*) In situ hybridization of whole-mount zebrafish embryos at 48 hpf with an antisense follistatin RNA probe. Arrowheads indicate regions expressing the follistatin gene in embryos injected at the one-cell stage with antisense MOs for *kdm7a* (5 ng) and *kdm7b* (5 ng) or with a control MO (10 ng). (*I*) The Tg(*HuC:Kaede*) embryos were injected at the one-cell stage with antisense MOs for follistatin (5 ng) or p53 (5 ng) genes or with a control MO (5 ng) in the indicated combinations. The morphology of the embryos at 48 hpf was examined by bright-field (*left* panels) or fluorescence (*right* panels) microscopy. Arrowheads indicate the tectum or presumptive tectal region.